Atmos. Chem. Phys. Discuss., 15, 30211–30267, 2015
www.atmos-chem-phys-discuss.net/15/30211/2015/
doi:10.5194/acpd-15-30211-2015

Atmospheric Chemistry and Physics Discussions

Theoretical study of mixing in liquid clouds – Part 1: Classical concept

A. Korolev[1], **A. Khain**[2], **M. Pinsky**[2], **and J. French**[3]

[1]Environment Canada, Cloud Physics and Severe Weather Section, Toronto, Canada
[2]Department of Atmospheric Sciences, the Hebrew University of Jerusalem, Jerusalem, Israel
[3]University of Wyoming, Laramie, WY, USA

Received: 17 August 2015 – Accepted: 5 October 2015 – Published: 4 November 2015

Correspondence to: A. Korolev (alexei.korolev@ec.gc.ca)

Published by Copernicus Publications on behalf of the European Geosciences Union.

Abstract

Relationships between basic microphysical parameters are studied within the framework of homogeneous and extreme inhomogeneous mixing. Analytical expressions and numerical simulations of relationships between droplet concentration, extinction coefficient, liquid water content, and mean volume droplet size, formed at the final stage of mixing are presented. The expressions are used to identify type of mixing for in-situ observations obtained in convective clouds. The analysis suggests that for the set of observations investigated here, the interaction between cloudy and entrained environments is dominated by inhomogeneous mixing. Lastly, an analysis of different response times of the cloud environment undergoing mixing is presented. Comparisons of different characteristic times suggest that within the same mixing environment depending on mixing fraction some volumes may be dominated by homogeneous mixing whereas others by inhomogeneous mixing.

1 Introduction

Turbulent mixing is an important non-adiabatic process in the atmosphere that to a large extent determines spatial gradients of many thermodynamic (e.g. temperature, humidity) and cloud microphysical parameters (e.g. hydrometeor concentrations, extinction coefficient, condensed water content) and as such needs to be properly described in numerical simulations of clouds and weather predictions. Entrainment and mixing occurs during the entire lifetime of a cloud and is active not only near cloud edges, but it is important throughout the whole cloud volume. Mixing of cloudy and entrained air results in changes to the shape of the droplet size distribution through partial droplet evaporation and can also lead to changes in droplet concentration through complete evaporation of some fraction of droplets. The shape of the droplet size distribution plays key role in the initiation of precipitation and radiative properties of clouds.

ACPD
15, 30211–30267, 2015

The treatment of mixing in numerical simulations of clouds and precipitation formation remains a challenging problem. Besides the issues related to the way to describe mixing in numerical schemes, there is a fundamental problem of identifying a scenario or path, that mixing events should follow. Since the pioneering works of Latham and Reed (1977) and Baker et al. (1980) two explicitly alternative scenarios of mixing were identified. In the first scenario the turbulent mixing rapidly stirs the environment unifying the fields of temperature and humidity. After that all of the droplets undergo partial evaporation under the same conditions. The result of this mixing is the droplet population with reduced sizes, but their total amount remains unchanged. This type of mixing is referred to as *homogeneous*. In the second scenario, mixing occurs more slowly such that the population of droplets experiences different amount of sub-saturation. Some number of droplets completely evaporates while others experience no evaporation until the entirety of the entrained air becomes saturated. After that turbulence mixes the rest droplets with the saturated environment. During this type of mixing the size of droplets remains unchanged; however, their concentration is reduced. This type of mixing is called *extreme inhomogeneous*. The intermediate case when some fraction of droplets evaporate partially, the other fraction evaporates completely, and the third fraction remains without changes in some works referred to as inhomogeneous (e.g. Baker and Latham, 1980).

The conditions for homogeneous and inhomogeneous mixing and their effects on precipitation formation have been debated in cloud physics over forty years. There are a number of numerical simulations and theoretical efforts on studying different aspects of mixing and its effect on cloud microphysics (e.g. Baker and Latham, 1982; Jensen and Baker, 1989; Su et al., 1989; Lasher-Trapp et al., 2005; Jeffrey, 2007; Andrejczuk et al., 2009; Kumar et al., 2013 and many others). A comprehensive review of the works on the effect of turbulence and mixing on cloud droplets formation can be found in Devenish et al. (2012).

A number of studies were dedicated to identifying type of mixing based on in-situ observations. Most of the previous in-situ observations provide evidence supporting inho-

ACPD
15, 30211–30267, 2015

mogeneous mixing (e.g. Hill and Choularton, 1985; Paluch, 1986; Bower and Choularton, 1988; Blyth and Latham, 1991; Gerber et al., 2008). However, works of Jensen and Baker (1989), Paluch and Baumgardner (1989), Burnet and Brenguier (2007), Lehmann et al. (2009) suggest occurrence of homogeneous mixing. So, at the moment it appears that both types of mixing may occur in liquid clouds. However, the environmental conditions resulting from one or the other type of mixing remain not well understood.

Early experimental work on identifying type of mixing from in-situ observations were based on the analysis of spatial variability of the shapes of individual droplet size distributions (e.g. Paluch and Knight, 1984; Paluch, 1986; Bower and Choularton, 1988). However, the effectiveness of this method involving analysis of overly large number of individual size spectra turned out to be quite low. Another technique utilized functional relationships between droplet concentration (N) and droplet radius (r), which is specific to each type of mixing. Thus, during inhomogeneous mixing the droplet size is expected to remain unchanged, whereas the concentration will vary. However, during homogeneous mixing the droplet size and concentration in cloud will be related to each other in a certain way, depending on the mixing fraction and the humidity of the entrained air. This fact was used in observational studies on identifying type mixing from "mixing diagrams" that related N and r for different regimes of mixing (e.g. Burnet and Brenguier, 2007; Gerber et al., 2008; Lehmann et al., 2009).

The use of the mixing diagrams to some extent facilitated identification of type of mixing. However, in many cases scatter in the relationships between N vs. r was too large, which hindered identifying the type of mixing (Burnet and Brenguier, 2007). To resolve this problem many researchers used other complementary measurements supporting identification of the type of mixing (e.g. Gerber et al., 2008; Lehmann et al., 2009).

Besides the effect on N and r the type of mixing is anticipated to manifest itself in relationships between other moments of the droplet size distribution, $f(r)$. With the exception of the work by Hill and Choularton (1985), who correlated concentration and

ACPD
15, 30211–30267, 2015

liquid water content, there have been few attempts to use any other microphysical parameters for identification of type of mixing.

In order to fill this gap, this study presents a theoretical analysis of relationships between different moments of $f(r)$ within the framework of homogeneous and extreme inhomogeneous mixing. The analysis is focused on the first four moments of $f(r)$ corresponding to the droplet concentration N (0th moment), integral radius $N\overline{r}$ (1st moment), extinction coefficient β (2nd moment) and liquid water mixing ratio q (3rd moment) and mean volume radius $\overline{r}_3$ (mixed 3rd and 0th moment). It is shown that the set of relationships obtained can be effectively used to identify the type of mixing from in-situ observations.

This paper constitutes the first in a series of three papers. The present paper considers the final stage of mixing based on the formal definitions of homogeneous and inhomogeneous mixing. The following two papers provide a detailed analysis of the time dependent processes during homogeneous (Pinsky et al., 2015a) and inhomogeneous (Pinsky et al., 2015b) mixing.

The present paper is arranged in the following way. Section 2 presents analysis of the analytical relationship between $N, N\overline{r}, \beta, q, \overline{r}_3$ and mixing fraction μ for the cases of homogeneous and inhomogeneous mixing. The results of numerical simulation of $N, \beta, q, \overline{r}_3$ formed after mixing are discussed in Sect. 3. Examples of relationship between $N, \beta, q, \overline{r}_3$ from in-situ observations are presented in Sect. 4. Section 5 presents analysis of characteristic response times of a cloud environment during homogeneous and inhomogeneous mixing. The concluding remarks are presented in Sect. 6.

2 Effect of mixing on microphysical variables

2.1 Phenomenological consideration

The conceptual diagrams of homogeneous and extreme inhomogeneous mixing are shown on Fig. 1. During the first stage of extreme inhomogeneous mixing the sub-

ACPD
15, 30211–30267, 2015

saturated parcel is engulfed into the cloudy environment (Fig. 1a1). Then, the droplets at the interface of the sub-saturated parcel and the cloud environment undergo complete evaporation until the air within the engulfed volume reaches saturation (Fig. 1a2). After that the saturated but droplet free parcel mixes with the rest of the cloud environment (Fig. 1a3). The result of the inhomogeneous mixing is that the cloud parcel has reduced droplet concentration and the droplet sizes remain unchanged.

In the case of homogeneous mixing after entraining into a cloud (Fig. 1b1), the sub-saturated parcel "instantly" mixes up with its cloud environment (Fig. 1b2), which leads to undersaturation of the total volume. Then, all droplets throughout the mixed volume undergo simultaneous evaporation until the equilibrium state is reached. The result of homogeneous mixing is a cloud parcel with reduced concentration of droplets and droplets with reduced sizes (Fig. 1b3).

The difference between these two types of mixing is as follows: in the case of inhomogeneous mixing the saturation is reached through complete evaporation of some fraction of droplets, whereas their sizes remain constant. In case of homogeneous mixing the saturation is reached through a uniform evaporation of droplets, whereas the total number of droplets in the diluted parcel remains unchanged. It should be noted that in both cases of mixing the droplet concentration decreases due to dilution by the entrained droplet free sub-saturated parcel.

The following discussion will be specifically focused at the microphysical properties formed at the final stage of the homogeneous and extreme inhomogeneous mixing. The processes occurring during mixing state (i.e. transition 1a→2a and 1b→2b in Fig. 1) remain outside the frame of this work. Following the formalism of homogeneous and inhomogeneous mixing, the process of mixing reaches the final stage when (1) the entrained and cloud environment are mixed up and the spatial gradients of the microphysical (N, β, q, etc.) and environmental (T, S, e, etc.) parameters approach to zero; (2) the diffusional process related to droplet evaporation comes into equilibrium. The second condition is completed when (a) the environment reaches saturation state,

ACPD
15, 30211–30267, 2015

or (b) the entire population of droplets is completely evaporated, if the mixed air is too dry.

The above description of homogeneous and inhomogeneous mixing is highly idealized. Broadwell and Breidenthal (1982) summarized the experimental evidence and proposed the following description of mixing in turbulent shear layers. Mixing takes place in a series of events. Two shear layers exchange mass by engulfing parcels from an opposite layer into localized zones. The initially large-scale filaments of the two gases break down towards smaller scales due to the action of turbulence. The turbulence stretches the interface between the gases and enhances the molecular diffusion across the increasing surface. The actual mixing of the engulfed volume is a molecular diffusion process that is most effective after the break down volumes reduce to the Kolmogorov viscosity scale. It is anticipated that the reaction of the ensemble of droplets from entrainment is a combination of homogeneous and inhomogeneous mixing with domination of one type of mixing over the other depending on the characteristic spatial and time scales of the environment determined by turbulence, cloud microphysics, state parameters and stage of mixing.

2.2 Methodology

The foregoing discussion will be focused on mixing between saturated cloud parcels and out-of-cloud sub-saturated air. The cloud parcel contains droplets with monodisperse radius r_0, liquid mixing ratio q_0 and number concentration N_0. The initial temperature in the cloud parcel is T_1, relative humidity $S_1 = 1$, where $S = e/E_s(T)$ (The explanation of variables notations is provided in Table A1). The second parcel is droplet free ($N_2 = 0$), sub-saturated with initial relative humidity $S_2 < 1$ and temperature T_2. The mixing occurs isobarically, i.e. during mixing p = const. At the end of the mixing the temperature and humidity formed in the resulting parcel are T_m and S_m (appendix). The process of mixing is completed when the mixed parcel reaches equilibrium due to the air saturation (i.e. $S_m = 1$), or due to the complete evaporation of droplets. In the latter case the final humidity is $S_m < 1$. The effect of the vertical velocity and vertical

ACPD
15, 30211–30267, 2015

travel of the mixing parcels on temperature T_m, humidity S_m, and condensed water q_m is not considered here, i.e. vertical velocity $u_z = 0$.

Without the loss of generality the masses of the cloudy and sub-saturated volumes prior to the mixing are assumed to have a unit masses, i.e. $m_1 = 1$ and $m_2 = 1$. The mixing process will be considered as mixing of the μ fraction of the cloud volume with the $(1 - \mu)$ fraction of the second (sub-saturated) volume. The mixing fraction is changing within the range of $0 \le \mu \le 1$. Therefore, the mass of the resulting mixed parcel is equal to $m_1\mu + (1 - \mu)\, m_2 = 1$. This approach simplifies the consideration of mixing and allows considering all possible proportions of the mixing of two volumes.

2.3 Extreme inhomogeneous mixing

Within the framework of the extreme inhomogeneous mixing some fraction of droplets undergo complete evaporation, whereas the rest of the droplets remain unchanged. Therefore, such process results in scaling the droplet size distribution $f(r)$, i.e.

$$f(r) = k f_0(r) \tag{1}$$

where k is some coefficient dependent on μ and the initial environmental parameters of the mixing volumes, $f_0(r)$ is the droplet size distribution before mixing.

Equation (1) yields relationship between pairs nth and mth moments

$$\frac{M_n}{M_{0n}} = \frac{M_m}{M_{0m}} \tag{2}$$

where $M_n = \int_0^\infty f(r) r^n \mathrm{d}r$ is the nth moment of $f(r)$. Therefore, it is anticipated that for inhomogeneous mixing droplet number concentration N (0th moment), extinction coefficient β (2nd moment), liquid water content q (3rd moment), along with other moments, will correlate with each other, i.e.

$$\frac{N}{N_0} = \frac{\beta}{\beta_0} = \frac{q}{q_0} \tag{3}$$

ACPD
15, 30211–30267, 2015

One of the consequences of Eqs. (1)–(3) is conservation of characteristic droplet sizes, i.e. $\overline{r}$, $\overline{r}_2$, $\overline{r}_3$, r_{eff} will remain constant during inhomogeneous mixing.

The liquid water mixing ratio q resulting from extreme inhomogeneous mixing can be written based on the mass balance of vapor and liquid water as

$$q = \mu q_0 - \delta q, \tag{4}$$

where δq is the amount of liquid water per 1 kg of the dry air required to saturate the volume formed as a result of mixing of the cloud and entrained parcels before droplet evaporation. The value of δq can be found as (appendix)

$$\delta q = \frac{L^2}{c_p R_v T_2^2} \ln\left(\frac{1 + \frac{E_s(T_{m0}) R_a L^2}{p c_p R_v^2 T_{m0}^2}}{1 + S_{m0} \frac{E_s(T_{m0}) R_a L^2}{p c_p R_v^2 T_{m0}^2}} \right) \tag{5}$$

Here T_{m0} and S_{m0} are the temperature and relative humidity formed in the parcel after mixing, but before droplets start evaporating (appendix), $E_s(T_{m0})$ is saturation humidity at temperature T_{m0}. Since T_{m0}, S_{m0} and E_s are functions of the ratio of μ, then δq is function of μ as well.

Combining Eqs. (4) and (3) yields dependence of N vs. μ

$$N = N_0 \left(\mu - \frac{\delta q}{q_0} \right) \tag{6}$$

Equations (4) and (5) describe changes of q and δq for a general case, when the temperatures in the cloud (T_1) and sub-saturated (T_2) parcels are different. When $T_1 = T_2$, the temperature after mixing, but before droplet evaporation, remain the same, i.e. $T_{m0} = T_1 = T_2$. For this case the amount of liquid water evaporated after mixing can be estimated as the amount of evaporated liquid required to saturate the entrained parcel

$$\delta q = (1 - \mu)\delta q^*, \tag{7}$$

ACPD
15, 30211–30267, 2015

where

$$\delta q^* = \frac{L^2}{c_p R_v T_2^2} \ln\left(\frac{1+\frac{E_S(T_2)R_a L^2}{pc_p R_v^2 T_2^2}}{1+S_2\frac{E_S(T_2)R_a L^2}{pc_p R_v^2 T_2^2}}\right) \quad (8)$$

is the amount of liquid water required to saturate 1 kg of the entrained sub-saturated volume. Therefore, Eq. (4) can be rewritten as

$$q = \mu q_0 - (1-\mu)\,\delta q^*, \quad (9)$$

Equation (8) does not take into account the air temperature changes due to the latent heat of droplet evaporation. The comparisons of with numerical simulations showed that the Eqs. (8) and (9) provide accuracy within few percent when the temperature difference $|T_1 - T_2| < 2\,^{\circ}\mathrm{C}$.

It should be noted that the mass balance Eqs. (4) and (9) do not take into account changes of the size of the volume V due to changes of temperature caused by evaporation of droplets. The temperature depression $\Delta T = |T_1 - T_2|$ due to evaporation depends onδq and it may reach a few degrees depending on μ and q_0 (Sects. 3.1 and 3.4). For isobaric processes the relative changes of volume can be estimated as $\frac{\Delta V}{V} = \frac{\Delta T}{T}$. So, for the lower troposphere $\Delta T = 1\,^{\circ}\mathrm{C}$, would result in a relative changes of volume less than 0.3 %. Therefore, the evaporative cooling within few degrees will not produce any significant effect on N, β and q during mixing, and the corrections of the volume changes can be neglected.

Similar to Eq. (6) the dependence of concentration vs. μ for the case $T_1 \approx T_2$ can be found as

$$N = N_0\left(\mu - \frac{(1-\mu)\delta q^*}{q_0}\right) \quad (10)$$

The dependences for other moments vs. μ for extreme inhomogeneous mixing can be found the same way as in Eqs. (6) or (10).

ACPD
15, 30211–30267, 2015

2.4 Homogeneous mixing

Based on mass conservation one may conclude that the amount of evaporated water does not depend on how the mixing occurred. Therefore, the mass balance equations (4) and (9) are valid for both homogeneous and inhomogeneous mixing.

For homogeneous mixing the droplet number concentration changes only due to dilution of the cloud parcel by the entrained air, i.e.

$$\frac{N}{N_0} = \mu \tag{11}$$

Assuming $T_1 \approx T_2$ and substituting Eq. (11) into (9) yields dependence q vs. N for homogeneous mixing:

$$\frac{N}{N_0} = \frac{q + \delta q^*}{q_0 + \delta q^*} \tag{12}$$

Equation (12) suggests linear relationship between N and q for homogeneous mixing. However, no linear relationships exist between other moments. Thus, substituting the definition of the liquid water ratio $q = 4\pi\rho_w N\overline{r}_3^3/3$ in Eq. (12) yields the relationship between changes of droplet size and concentration

$$\frac{\overline{r}^3}{\overline{r}_{30^3}} = 1 + \frac{\delta q^*}{q_0}\left(1 - \frac{N_0}{N}\right) \tag{13}$$

In a similar way the relationship between the extinction coefficient $\beta = Q\pi N\overline{r}_2^2$, concentration and liquid water can be obtained as

$$\frac{\beta}{\beta_0} = \frac{N}{N_0}\left(1 + \frac{\delta q^*}{q_0}\left(1 - \frac{N_0}{N}\right)\right)^{2/3} \tag{14a}$$

$$\frac{\beta}{\beta_0} = \frac{q}{q_0}\left(\frac{q + \delta q^*}{q_0 + \delta q^*}\right)^{5/3} \tag{14b}$$

ACPD
15, 30211–30267, 2015

In Eqs. (14a) and (14b) it is assumed that $\overline{r}_2 \approx \overline{r}_3$[1].

Substituting in Eq. (13) the expression for the time of phase relaxation (e.g. Korolev and Mazin, 2003)

$$\tau_p = \frac{1}{bN\overline{r}} \tag{15}$$

and assuming $\overline{r} \approx \overline{r}_3$, yields

$$\frac{\tau}{\tau_0} = \frac{N_0}{N}\left(1 + \frac{\delta q^*}{q_0}\left(1 - \frac{N}{N_0}\right)\right)^{1/3} \tag{16}$$

For the cases when the temperature difference $|T_1 - T_2|$ exceeds a few degrees, the effect of μ on T_m and S_m should be taken into consideration in the calculations of evaporated water. For such cases δq (Eq. 5) should be used instead of δq^* (Eq. 8). Using Eq. (11) δq can be presented as a function of $\frac{N}{N_0}$, i.e. $\delta q(\mu) = \delta q\left(\frac{N}{N_0}\right)$. Replacing Eq. (9) by (4) in the above consideration, the equations Eqs. (12)–(14), and (16) can

[1]Equalities $\overline{r}_2 \approx \overline{r}_3$ and $\overline{r} \approx \overline{r}_3$ are valid for a relatively narrow droplet size distributions.

ACPD
15, 30211–30267, 2015

be rewritten as

$$\frac{N}{N_0} = \frac{q + \delta q\left(\frac{N}{N_0}\right)}{q_0} \tag{17}$$

$$\frac{\bar{r}_{3^3}}{\bar{r}_{30^3}} = 1 - \frac{\delta q\left(\frac{N}{N_0}\right)}{q_0}\frac{N_0}{N} \tag{18}$$

$$\frac{\beta}{\beta_0} = \frac{N}{N_0}\left(1 - \frac{\delta q\left(\frac{N}{N_0}\right)}{q_0}\frac{N}{N_0}\right)^{2/3} \tag{19}$$

$$\frac{\beta}{\beta_0} = \frac{q^{1/3}\left(q + \delta q\left(\frac{\beta}{\beta_0}\right)\right)^{2/3}}{q_0} \tag{20}$$

$$\frac{\tau_{\mathrm{p}}}{\tau_{\mathrm{p0}}} = \frac{N_0}{N}\left(1 - \frac{\delta q\left(\frac{N}{N_0}\right)}{q_0}\frac{N_0}{N}\right)^{-1/3} \tag{21}$$

Equations (17)–(21) are non-linear and can be solved numerically.

2.5 Complete evaporation

The amount of evaporated water is determined by the initial and final values of the state parameters (e.g. T, e, p) in the mixed parcel, and it does not depend on the type of mixing. Therefore, Eqs. (4) and (9) are valid for both homogeneous and inhomogeneous mixing.

For the general case when $T_1 \neq T_2$ the value of δq is a function of μ, i.e. $\delta q(\mu)$ (Eq. 5). Then, in order to find the critical value of μ_{cr}, when all liquid water evaporates

ACPD
15, 30211–30267, 2015

(i.e. $q = 0$) a non-linear equation should be solved

$$\mu_{cr} q_0 - \delta q(\mu_{cr}) = 0 \tag{22}$$

If the temperature of the entrained and cloud parcels are the same (i.e. $T_1 = T_2$), then the critical mixing fraction for the case $q = 0$ can be computed from Eq. (9) as

$$\mu_{cr} = \frac{\delta q^*}{q_0 + \delta q^*} \tag{23}$$

Equation (23) yields the condition for the mixing fraction of entrained and cloud parcels such that if $\mu < \mu_{cr}$ then all liquid water in the parcel after completing the mixing evaporates ($q = 0$).

Figure 2 shows comparisons of dependences of μ_{cr} vs. q_0 for different S_0 calculated from Eq. (23) and those deduced from a numerical model. As it is seen the agreement appeared to be reasonably good.

Critical ratios of mixing are also shown by black stars in Fig. 4a and b (Eq. 23). As seen from Fig. 4a and b the locations of the black stars coincide well with the locations where modeled LWC and N become zero. The obtained agreement between analytical and modeled μ_{cr} in Figs. 3 and 4 validates the developed approach.

3 Modeling

Numerical simulations of the final stages of homogeneous and inhomogeneous mixing were performed in order to examine the accuracy and limitations of the analytical expressions obtained in the previous section. The simulations have been conducted with the help of a parcel model similar to that described in Korolev (1995). The ensemble of droplets in the simulation was assumed to be monodisperse.

For the case of inhomogeneous mixing the amount of evaporated water Δq required to saturate the mixed volume was calculated first. If $\Delta q < q_0$, then the concentration

ACPD
15, 30211–30267, 2015

of evaporated droplets was calculated as $N_{ev} = \frac{\Delta q}{\overline{m}_d}\rho_a$, where $\overline{m}_d = 4\pi\rho_w\overline{r}_3^3/3$ is the average mass of a droplet. Then the concentration of the remaining droplets $N = N_0 - N_{ev}$ was recalculated based of the calculation on the volume formed after mixing. If $\Delta q \geq q_0$, then all droplets evaporate and $N = 0$.

For the case of homogeneous mixing in the first step the engulfed parcel instantly mixes with the cloud parcel resulting in a new humidity S_{m0}, temperature T_{m0} and volume V_{m0}. Then the droplets start evaporating until either their complete evaporation or saturation over liquid is reached. The calculations stopped when, either $r < 0.1$ µm or $(E_S - e)/E_S < 0.001$, respectively.

3.1 Effect of mixing ratio

Figure 3 shows the results of the simulation of the dependence of the droplet number concentration (N), droplet integral radius ($N\overline{r}$), extinction coefficient (β), liquid water mixing ratio (q) mean cube droplet radius ($\overline{r}_3$), and time of phase relaxation (τ_p), relative humidity (S_{m0}, S_m) and final temperature (T_m) vs. mixing fraction μ. The calculations were performed for different saturation ratios of the entrained parcel $S_{20} = 0.2$, 0.5, 0.8 and 0.95. As seen from Fig. 3 for the case of homogeneous mixing only N and q are linearly related with μ, the rest of the variables have non-linear dependences on μ. For the case of inhomogeneous mixing all $f(r)$ moments and droplet size linearly depend on the mixing fraction when $\mu > \mu_{cr}$. When $\mu \leq \mu_{cr}$ all liquid evaporates. Since the amount of the evaporated liquid water does not depend on the type of mixing, the dependences of $q(\mu)$ are the same for both homogeneous and inhomogeneous mixing (Fig. 3a). The type of mixing has the most pronounced effect on the droplet concentration (Fig. 3b) and droplet sizes (Fig. 3e). The obtained results are in a good agreement with the analytical predictions discussed in Sect. 2.

Figure 3g shows the dependences $S_{m0}(\mu)$ and $S_m(\mu)$. Here $S_{m0}(\mu)$ is humidity at the initial stage of homogeneous mixing before droplets start evaporating (Fig. 1b2). Figure 3h presents dependences of $T_m(\mu)$ for different S_2. It is worth noting that $S_m(\mu)$

ACPD
15, 30211–30267, 2015

and $T_m(\mu)$ do not depend on the type of mixing and they are the same for homogeneous and inhomogeneous mixing. Basically the independence of $q(\mu)$, $S_m(\mu)$ and $T_m(\mu)$ on type of mixing is the consequence of the mass and energy conservation laws, which are not contingent on type of mixing.

3.2 Effect of humidity

The diagrams in Fig. 4 show the dependences of normalized β, q and $\overline{r}_3$ vs. N/N_0 calculated from numerical simulations and analytical equations from Sect. 2. The calculations were performed for different humidity of the entrained air S_2. As seen from Fig. 4, the normalized dependences $q(N)$, $\beta(N)$ and $\overline{r}_3(N)$ tend to approach the line of inhomogeneous mixing when relative humidity S_2 approaches to 100 %. As it was indicated in previous studies (e.g. Burnet and Brenguier, 2007), mixing with the entrained saturated air ($S_2 = 1$) represents of degenerate case, when there is no difference between homogeneous or inhomogeneous mixing. In this case droplets behave as a passive admixture and they do not interact with the environment. This effect is clearly seen from the diagrams in Fig. 4.

3.3 Effect of liquid water content

Figure 5 presents the normalized dependences $q(N)$, $\beta(N)$ and $\overline{r}_3(N)$ calculated for different initial liquid water q_0 in the cloud parcel, but the same humidity of the entrained parcel $S_2 = 0.5$. Figure 5 shows that the increase of q_0 results in $q(N)$, $\beta(N)$ and $\overline{r}_3(N)$ (which were calculated for homogeneous mixing) approaching towards $q(N)$, $\beta(N)$ and $\overline{r}_3(N)$ for the inhomogeneous mixing. In other words, the sensitivity of the microphysical parameters to the type of mixing increases with the decrease of q_0. From a practical viewpoint it means that from in-situ observations the difference between homogeneous and inhomogeneous is anticipated to be more pronounced for the cases with a relatively low LWC ($q_0 < 1\,\mathrm{g\,m^{-3}}$).

ACPD
15, 30211–30267, 2015

3.4 Effect of temperature

Figure 6 shows the effect of temperature on the normalized dependences $q(N)$, $\beta(N)$ and $\overline{r}_3(N)$ calculated for the case $T_1 = T_2$. The relative humidity of the entrained parcel was assumed to be the same for all cases ($S_2 = 0.5$). Figure 6 suggests that the difference between the $f(r)$ moments becomes most pronounced at warm temperatures, whereas at cold temperatures (e.g. $T = -30\,^{\circ}\mathrm{C}$) $q(N)$, $\beta(N)$ and $\overline{r}_3(N)$ are approaching the inhomogeneous mixing limit.

Such behavior is explained by the fact that the amount of liquid water deficit δq decreases with decreasing temperature. The effect of T on δq is demonstrated in Fig. B1 (appendix). At low temperatures ($T < -30\,^{\circ}\mathrm{C}$) the amount of evaporated water δq is so small, that homogeneous mixing with undersaturated out-of-cloud air will have approximately the same effect as mixing with saturated air (i.e. degenerate case).

It is well established that isobaric mixing of two saturated parcels having different temperatures results in the formation of supersaturated air (e.g. Rogers, 1976; Bohren and Albrecht, 1998). However, as it was shown in Korolev and Isaac (2000), the isobaric mixing of saturated cloudy and undersaturated air may also result in supersaturated air. The formation of supersaturated air leads to different dependences between $N\overline{r}$, β, q, $\overline{r}$ and N as compared to those shown in Figs. 3–6 when $T_1 = T_2$. In the cases discussed above, mixing between cloud and sub-saturated entrained air with $T_1 = T_2$ resulted in evaporation of some fraction of cloud liquid water, i.e. it was always $\delta q < 0$. However, mixing that causes supersaturation will result in condensation of liquid water (e.g. $\delta q > 0$), which is different of the cases considered above.

Figure 7 presents a set of diagrams similar to those in Fig. 3, but calculated for the cloud and entrained sub-saturated parcels having different temperatures T_1 and T_2. It turns out that for the case of inhomogeneous mixing the temperature difference between T_1 and T_2 breaks down linear dependences between μ and $f(r)$ moments (e.g. $N\overline{r}$, β, q, Fig. 7a–c). This happens because positive supersaturation ($S_{m0} > 1$), which may form after mixing, will result in an increase of q, β, $\overline{r}_3$, etc. The droplet

ACPD
15, 30211–30267, 2015

concentration still holds the linear relationship with μ (Fig. 7b), since no formation of new droplets were allowed when $S_{m0} > 1$.

Figure 8 presents the effect of the temperature difference ΔT on the normalized dependences $q(N)$, $\beta(N)$ and $\overline{r}_3(N)$. As seen from Fig. 8 for large temperature differences $\Delta T = 10\,^{\circ}\mathrm{C}$, the values of q, β, $\overline{r}$ for inhomogeneous mixing exceed those for inhomogeneous mixing for the same concentration N.

It is worth nothing that in real clouds, high supersaturation resulting from isobaric mixing may lead to activation of interstitial CCN, which may slow down the growth of $\overline{r}_3$ and increase N (Korolev and Isaac, 2000). However, no activation of new droplets during isobaric mixing was allowed in this study. For the cases when $S_{m0} > 1$ (Fig. 8, section AB on line 1) the condensed water was uniformly distributed between available droplets, and therefore, $q(N)$, $\beta(N)$ and $\overline{r}_3(N)$ calculated for homogeneous and inhomogeneous mixing to coincide with each other.

Numerical simulations also showed, that the effect of temperature on the result of mixing is more pronounced for the cases when the cloud temperature is warmer than that of the entrained air, i.e. $T_1 > T_2$, as compared to the cases with $T_1 < T_2$.

3.5 Multiple mixing events

In the previous sections the mixing between cloud and sub-saturated volumes was considered as a single event. Such mixing will be referred to as "primary" mixing. Primary mixing results in an ensemble of elementary volumes characterized by a set of microphysical and state parameters i.e. $\overline{r}(\mu)$, $N(\mu)$, $S(\mu)$, $T(\mu)$, etc. Each of these parameters has a functional dependence on μ, and what is important, these parameters have functional relationships between each other.

In reality mixing is a continuous process. It does not stop after the primary mixing. The elementary volumes formed after primary mixing continue progressively mixing between each other, cloud environment and newly entrained air.

ACPD
15, 30211–30267, 2015

The second stage of mixing will result in an ensemble of elementary volumes characterized by a set of parameters $\overline{r}^{(2)}$, $N^{(2)}$, $S^{(2)}$, $T^{(2)}$, etc. Here the superscript $^{(2)}$ indicates the stage of mixing. After the second stage the mixed volumes undergo subsequent stages of mixing. The conceptual diagram of the progressive mixing is shown in Fig. 9. This is a highly idealized scheme of mixing. However, it helps understand some features of homogeneous mixing.

The progressive mixing was simulated with the help of a numerical model, where parcels were randomly mixed with each other and with the cloud environment. The mixing fraction μ was also set to be random during each mixing event. Models of random mixing have been used in a number of studies (e.g. Krueger et al., 1997; Su et al., 1998; Burnet and Brenguier, 2007). Burnet and Brenguier (2007) allowed mixing between cloud and entrained parcels at each stage of mixing. In the present approach the mixing with the entrained environment was allowed only at the primary stage. After that the mixing continued with the cloud air and between the mixed volumes.

The results of the progressive mixing for the first four stages are presented in Fig. 10. As seen from Fig. 10 the functional relationship between the pairs of microphysical and state parameters exists only for the primary stage. However for higher mixing stages these functional relationships breakdown. Thus, cloud volumes with the same $N^{(2)}$ will be associated with an ensemble of droplets with different $\overline{r}^{(2)}$. Figure 10 also shows the regions of scattering of $q(N)$, $\beta(N)$ and $\overline{r}_3(N)$ for stages 2, 3 and 4 are limited from above by the inhomogeneous mixing (red dashed lines) and from below by primary homogeneous mixing (red solid lines). During the progressive mixing $N^{(n)}\beta^{(n)}$, $q^{(n)}$ and $\overline{r}_3^{(n)}$ formed in the elementary parcels tend to approach those in the undiluted cloud, i.e. N_0, β_0, q_0 and $\overline{r}_{30}$. This process can be considered as a surrogate to the diffusion process between the cloud and sub-saturated out-of-cloud environment. The convergence of $N^{(n)}\beta^{(n)}$, $q^{(n)}$ and $\overline{r}_3^{(n)}$ during the progressive mixing can be seen in Fig. 10, where the scattering of normalized $q^{(n)}(N)$, $\beta^{(n)}(N)$ and $\overline{r}_3^{(n)}(N)$ becomes denser towards the top-right corner (1,1) with the increase of the stage of mixing.

ACPD
15, 30211–30267, 2015

Another interesting feature of the progressive homogeneous mixing is that it results in a population of points along the line corresponding to inhomogeneous mixing (dashed red line in Fig. 10) In other words during homogeneous mixing some fraction of elementary volumes may develop properties of inhomogeneous mixing. Similar conclusion was derived from a more comprehensive analysis of mixing in Pinsky et al. (2015b).

As follows from Eq. (1) for the case of inhomogeneous mixing the progressive mixing does not affect the functional relations between $N^{(n)}\beta^{(n)}$, $q^{(n)}$, $\overline{r}_3^{(n)}$ and other microphysical parameters. These relations remain the same regardless of the actual stage of mixing. This is one of the fundamental differences between homogeneous and inhomogeneous mixing, which can be used for identification of type of mixing from in-situ measurements.

3.6 Droplet size distribution

Figure 11 shows modeled droplet size distributions averaged over an ensemble of elementary volumes corresponding to first four stages of homogeneous mixing. As seen from Fig. 11a–d for the case with $T_1 = T_2$ the droplet size distributions are broaden towards small sizes. Broadening of the droplet size distribution during homogeneous mixing is well known and it was demonstrated in a number of studies (e.g. Baker and Latham, 1982; Jensen and Baker, 1989; Kumar et al., 2013). However, if the difference $|T_1 - T_2|$ exceeds few degrees and the humidity of the sub-saturated parcel is not too low (e.g. $\geq 80\,\%$), then homogeneous mixing may result in supersaturation of the mixed parcel and subsequent droplet growth. In this case the droplet size distribution may broaden towards large sizes (Fig. 11e–h).

The examples in Fig. 11 show that homogeneous mixing results in broadening of size distribution. Depending on the temperature difference $|T_1 - T_2|$ and the relative humidity of the entrained air the broadening may occur both towards smaller and towards larger sizes. Contrary to homogeneous mixing, extreme inhomogeneous mixing does not result in broadening of droplet size distributions.

ACPD
15, 30211–30267, 2015

These results were obtained in the frame of the formalism of homogeneous and inhomogeneous mixing. The following two works in this series (Pinsky et al., 2015a, b) show that $f(r)$ broadening towards small droplets may occur during both homogeneous and inhomogeneous mixing.

3.7 Summary

In this section we summarize how homogeneous and inhomogeneous mixing is expected to manifest itself in relationships between basic microphysical parameters, such as N, β, q and $\overline{r}_3$. The objective of this analysis is to facilitate examination of in-situ measurements in order to identify the type of mixing within the conventional framework of homogeneous and extreme inhomogeneous mixing.

Following inhomogeneous mixing the relationship between the pairs of N, β and q are determined by a linear relationship $M_n = \alpha_{nm} M_m$ (Eq. 2). As follows from Eq. (3) the slopes α_{nm} for $q(N)\beta(N)$ and $q(\beta)$ are equal to the ratios q_0/N_0 β_0/N_0 and q_0/β_0. For clouds forming through vertical motions (e.g. Sc, Ac, Cu, Cb etc.) N_0, β_0 and q_0 correspond to undiluted adiabatic values. The values of N_0, β_0 and q_0 depend of the location of measurements and the environmental conditions at the cloud base. Thus the adiabatic value of q_0 is a function of elevation above the cloud base ΔZ. The concentration N_0 depends on the vertical velocity at the cloud base u_z and the aerosol load. The extinction coefficient β_0 is determined by both ΔZ and u_z. Therefore, for the measurements collected in the same cloud, but at different altitudes, it is anticipated that the scattering of N_0, and q_0 will be limited by a sector as shown in Fig. 12a. The scattering of measurements $q(N)$ will be aligned along an ensemble of different lines associated with different q_0/N_0. The conceptual diagram of the scattering of $q - N$ measurements in a cloud having experienced extreme inhomogeneous mixing is shown in Fig. 12a. The scatter diagrams of $q - \beta$ and $N - \beta$ will have the same patterns as that in Fig. 12a.

For the case of homogeneous mixing the functional relationship between the pairs of N, q, β and $\overline{r}_3$ is disrupted by a progressive mixing. As shown in Sect. 3.5 the

ACPD
15, 30211–30267, 2015

ensemble of points of Nq, and β will be scattered within a sector, which is limited by lines determined by Eq. (3) (inhomogeneous mixing) and Eqs. (12), (13) and (14a) (primary homogeneous), respectively (Fig. 10). What is important, is that the top of the cones of the scatter plots $q(N)$ and $\beta(N)$ correspond to points $[N_0, q_0]$ and $[N_0, \beta_0]$, respectively. Since N_0, β_0 and q_0 may vary both within the same cloud as well as from cloud to cloud, it is anticipated that the Nq, and β measurements will be scattered within an ensemble of cones as shown in Fig. 12b.

In the case of inhomogeneous mixing, which occurs within a cloud volume with the same N_0 and q_0, the scattered points are aligned along the same line, e.g. $q = \frac{q_0}{N_0} N$. Such scattering patterns are easy to identify even when there are a limited number of measured points. However, in the case of homogeneous mixing the points will be scattered within a large area limited by the cone with the top point $[N_0, q_0]$ (Fig. 12b). Even in case of a relatively large number of measurements the identification of such scattering patterns may be hindered because of the low density of points scattered over a large area. Ultimately, when looking at the feasibility of identifying homogeneous and inhomogeneous mixing by means of microphysical measurements it can be concluded that, when using the analysis of scatter-diagrams $q(N)$, $\beta(N)$ and $q(\beta)$, inhomogeneous mixing is easier identify than homogeneous mixing.

4 In-situ observations

This section presents an attempt to identify type of mixing based on examining relationships between basic microphysical parameters N, β, LWC, $\overline{r}_3$ measured from in-situ. These parameters present different moments of droplet size distribution and depending on instrumentation set used airborne, they can be either measured directly or calculated from measurements of $f(r)$.

ACPD
15, 30211–30267, 2015

4.1 Results of observations

The measurements were obtained on the University of Wyoming King Air aircraft during the COPE-MED project in South-Western part of UK during July-August 2013 (Leon et al., 2015). The UW King Air was equipped with a suite of microphysical instruments, including a DMT Cloud Droplet probe (CDP) and PMS Forward Scattering Spectrometer Probe (FSSP-100). These probes were designed for measurements of droplet sizes and their concentrations in the nominal size ranges 1–50 µm and 3–47 µm, respectively.

The measurements were focused on characterizing microphysical evolution of convective clouds and effect of entrainment on precipitation formation. Figure 13 shows a time series of droplet concentration, extinction coefficient, liquid water content and mean volume droplet diameter measured by the CDP during transit through a convective cell on 18 July 2013. The CDP data were sampled at 10 Hz, which corresponds to approximately 10 m spatial averaging. Visual examination of the spatial changes of N, β and LWC shows strong correlation. The amplitude of changes of these parameters reaches nearly one hundred percent with respect to their maximum. Contrary to that, the spatial variations of $\overline{D}$ and $\overline{D}_3$ are quite conservative and their values remain nearly constant. With the exception of two cloud holes between 13:50:42 and 13:50:44, the amplitude of fluctuations of $\overline{D}_3$ does not exceed 8 % with standard deviation of 2.2 %.

Figure 14 shows scatter diagrams of LWC(N), $\beta(N)$, LWC(β) and $\overline{D}_3(N)$ measured by the CDP during seven consecutive penetrations of the same convective cell extended over a period of approximately 19 min. One of these penetrations is shown in Fig. 13. The measurements were conducted at an altitude H = 5500 m and temperature $T = -12\,^{\circ}\mathrm{C}$. The relative humidity of the ambient air was approximately 20 %. At the beginning of the sampling no precipitation size particles were observed in the cloud. However, by the end of the sampling period some raindrops and ice crystals were present in the cloud. Despite the presence of some precipitation size particles, the scatter diagrams in Fig. 14a, b and d demonstrate high correlation between pairs N, β and LWC. The mean volume diameter in Fig. 14c shows very little changes from 19 to 17 µm

ACPD
15, 30211–30267, 2015

when concentration changes from 1100 to 500 cm^{-3}, However, for $N < 200\,cm^{-3}$, the volume diameter decreases to 12–15 µm.

Red lines in Fig. 14 indicate $q(N)$, $\beta(N)$, LWC(β) and $\overline{D}_3(N)$calculated for the 1st stage of homogeneous mixing. The calculations were performed for a monodisperse $f(r)$ with $D_0 = 18.5\,\mu m$ and $N_0 = 1100\,cm^{-3}$. The initial state parameters were considered to be the same as during the measurements. Comparisons of dependences $q(N)$, $\beta(N)$, $LWC(\beta)$ and $\overline{D}_3(N)$ based on in-situ measurements with those obtained from numerical simulations of homogeneous mixing show minor difference for high concentrations $500\,cm^{-3} < N < 1100\,cm^{-3}$ (Fig. 14a–c). Simulation shows that for this specific case the difference between homogeneous and inhomogeneous mixing does not exceed 10 % when $500\,cm^{-3} < N < 1100\,cm^{-3}$. Such difference remains within the errors of measurements. Therefore, in this specific cloud for the regions with $N > 500\,cm^{-3}$ the type of mixing cannot be unambiguously identified from the analysis of the dependences $q(N)$, $\beta(N)$, LWC (β) and $\overline{D}_3(N)$. However, for the regions with $N < 500\,cm^{-3}$ the deviation between homogeneous simulation and in-situ measurements becomes well pronounced and it extends beyond possible errors of measurements. This suggests that the mixing is in these regions is dominated by the inhomogeneous type.

Figure 15 shows the same type of diagrams as in Fig. 14, which were measured during 45 consecutive traverses through an ensemble of deep convective cells. The sampling altitude varied in the range $3000\,m < H < 4500\,m$, temperature $-11\,^{\circ}C < T < 0\,^{\circ}C$, relative humidity in the vicinity of clouds 15 %< RH < 65 %. The cloud measurements were extended over a period of 2 h 13 m, which is suggestive that the convective cells were sampled at different stages of their lifetime. At the sampling level the concentration of raindrops varied from zero to few per liter, and their diameter did not exceed 2 mm.

What is interesting that the scattering of the measurements LWC(N), $\beta(N)$ and LWC(β) (Fig. 15a, b and d) is limited by the sector, which originates from the zero point. Analysis showed that scatter diagrams LWC(N), $\beta(N)$, LWC(β) and $\overline{D}_3(N)$ cal-

ACPD
15, 30211–30267, 2015

culated for each individual cloud are very similar to those in Fig. 14. It appeared that the slopes of LWC(N), $\beta(N)$, LWC(β) vary from cloud to cloud. So, after averaging over the ensemble of clouds, the area of the scattered points will be located inside a sector limited by the lines with smallest and largest slopes.

As follows from Eq. (3) the slopes of $q(N)$, $\beta(N)$ and $q(\beta)$ are governed by the ratios q_0/N_0, β_0/N_0 and q_0/β_0, respectively, where N_0, β_0 and q_0 correspond to undiluted adiabatic values. As discussed in Sect. 3.7 changes in β_0 and q_0 can be explained by (a) different altitude of measurements above the cloud base, or (b) different cloud base temperatures in different clouds measured during this day. The changes in N_0 can be caused by (a) different vertical velocities u_z at the cloud base in different clouds, or (b) spatial and temporal changes of the aerosol load during measurements. The latter two causes will lead to different concentration of activated CCN. The combination of the above reasons may result in different slopes q_0/N_0, β_0/N_0 and q_0/β_0, which may be the reason of the scattering patterns of LWC(N), $\beta(N)$ and LWC(β) in Fig. 15.

A distinguishing characteristic of homogeneous mixing is that during evaporation the concentration tends to approach a non-zero value (Figs. 4–6), whereas during inhomogeneous mixing it approaches zero. The above analysis of the type of dependences LWC(N), $\beta(N)$, LWC(β) and $\overline{D}_3(N)$ in Figs. 14 and 15 clearly shows $N \rightarrow 0$, when $q \rightarrow 0$. This is another argument in favor that the mixing was dominated by inhomogeneous type.

4.2 Limitations of identifying type of mixing from in-situ measurements

Identification of type of mixing from in-situ observations is based on examination of relationships between moments of the size distributions measured along the flight path. The basic assumption underlying this analysis is that the cloud droplets in each averaging interval originate at the same altitude. Otherwise, the effects of mixing on size distributions will be superimposed with other processes affecting size distributions, which may affect the relationships between the microphysical parameters. Precipitating particles along with the presence of ice may also change the droplet number concentration

ACPD
15, 30211–30267, 2015

and liquid water content and therefore will affect the relationship between the moments. Altogether it limits the type of clouds suitable for examining homogeneous and inhomogeneous mixing. The most suitable candidates for that matter are non-precipitating convective clouds and stratocumulus clouds. However, as it was seen from above, high correlation between N, β and q may exist even in presence of small amounts of precipitation size particles.

Another limitation is based on the assumption that the sampled cloud parcel is in equilibrium state and that it reached the final stage of mixing. It is possible that during mixing the cloud mixed with the entrained air, but at the moment of measurement it remained undersaturated and the droplets did not complete changing their sizes. In this case the relationship between different moments may be well described as $M_n = \alpha_{nm} M_m$ and the mixing be confused with inhomogeneous mixing. In order to identify cases like this, accurate high frequency measurements of relative humidity are required. Unfortunately such measurements were not available during the in-situ observations described above.

Another limiting factor is that the above consideration did not account for the effect of the vertical velocity. The vertical changes of the relative humidity in adiabatic parcels are described by the equation (Korolev and Field, 2008)

$$\frac{1}{S}\frac{\mathrm{d}S}{\mathrm{d}z} = a \tag{24}$$

After linearization of its solution Eq. (24) yields the distance between the level with S_0 and saturation level ($S = 1$):

$$\Delta z = \frac{1 - S_0}{a} \tag{25}$$

According to Eq. (25) gives the relative humidity changes 10 % for $\Delta z \approx 200$ m at $T = 0\,^{\circ}$C. After reaching saturation the mixing turns into a degenerate case, which will appear as inhomogeneous mixing. Joint effects of evaporating droplets and an increase

ACPD
15, 30211–30267, 2015

in S during the vertical ascent may facilitate reaching saturation state. This case may be specifically relevant to the convective cloud measurements described above.

5 Characteristic time scales

The relative roles of mixing and evaporation is characterized by the Damkölher number (Dimotakis, 2005)

$$Da = \frac{\tau_{\text{mix}}}{\tau_{\text{react}}} \tag{26}$$

where τ_{mix} is the characteristic time of turbulent mixing; τ_{react} is the characteristic time of interaction of droplets with the environment through a molecular diffusion. The two extremes with $Da \gg 1$ and $Da \ll 1$, correspond to homogeneous and inhomogeneous mixing.

Over the years, the definition of the reaction time scale τ_{react} was debated in literature on mixing. In some studies τ_{react} was associated with the evaporating time of a droplet (e.g. Latham and Reed, 1977; Baker and Latham, 1979; Burnet and Brenguier, 2007; Andejchuk et al., 2009).

$$\tau_{\text{ev}} = \frac{F r_0^2}{S-1} \tag{27}$$

Another group of works considered that τ_{react} is equal to time of phase relaxation τ_{p} (Eq. 15) (e.g. Baker and Latham, 1982; Jeffery and Reisen, 2006; Kumar et. al. 2013). To compromise these two alternatives Jensen and Baker (1989), Jeffery (2007) considered both τ_{ev} and τ_{p}.

In the aforementioned studies in the estimations of τ_{react} the values of S (Eq. 27) r and N (Eq. 15) were assumed to be constant. However, none of these parameters remain constant during mixing. Thus, Lehman et al. (2009) pointed out that during

ACPD
15, 30211–30267, 2015

evaporation the population of droplets is interacting with the environment, and therefore $S(t)$ does not remain constant. They proposed considering τ_{react} as a "dominant" time of either evaporation of population of droplets (τ_{ev}) or time required for saturation of the cloud environment (τ_{eq}).

In reality the complete evaporation of droplets will be characterized by an ensemble of different τ_{ev}, rather than by a single value. The following two conditions should be satisfied for complete evaporation of a droplet: (1) the volume associated the droplet should be $\Delta V > \upsilon$, where

$$\upsilon = \frac{4\pi\rho_w r^3}{3\rho_a \delta q^*} \tag{28}$$

is the volume of the air, which will be saturated during a complete droplet evaporation; (2) the residence time of the droplet in the volume ΔV should be $\Delta t > \tau_{ev}$. The volume υ in fact is a minimum volume required for droplet evaporation, which means that the droplet evaporating time t_{ev} will be overly long. If the local concentration of the droplets is sparse enough, so that $\Delta V \gg \upsilon$, then the effect of the evaporating water on the humidity in ΔV can be neglected and it can be assumed that the local saturation ratio S = const during $t_{ev} \approx \tau_{ev}$.

Table 1 shows the calculated evaporating time (t_{ev}) and evaporating distance of the free falling droplet (λ_{ev}), size of the volume (λ_υ) saturated by a completely evaporated droplet with radius r at saturation ratio S. The size of the volume $\lambda_{\Delta V}$ required for evaporation of a single droplet should exceed its evaporating distance and saturating droplet volume, i.e.

$$\lambda_{\Delta V} > \lambda_{ev} \quad \text{and} \quad \lambda_{\Delta V} \gg \lambda_\upsilon. \tag{29}$$

Table 1 demonstrates that, depending on S and r, the value of $\lambda_{\Delta V}$ may vary from 10^{-2} cm to few cm. It appears that high humidity S and large r are strong factors limiting complete droplet evaporation, and therefore, declining inhomogeneous mixing.

ACPD
15, 30211–30267, 2015

Figure 16 shows τ_{ev} (black solid line) calculated for $S = S_{m0}$ assuming that S remains constant during its evaporation (i.e. single droplet evaporation). This case corresponds to homogeneous mixing, i.e. when turbulent eddies mixed the entrained environment prior droplets start evaporating. As seen, τ_{ev} is a strong function of μ. The smallest value of the evaporating time τ_{ev0} corresponds to unmixed entrained air $S = S_2$ at $\mu = 0$. Due to the fact that during mixing the saturation ratio varies in the range $S_2 < S < 1$, the evaporating time will change in the range $\tau_{ev0} < \tau_{ev} < \infty$. In other words τ_{ev0} presents the shortest evaporation time of a single droplet corresponding to S_2 of the entrained air.

It should be noted that complete evaporation of the entire population of droplets will occur when $\mu \le \mu_{cr}$ regardless type of mixing. The region of complete evaporation calculated for a population of droplets is shown on the left side of Fig. 16 in section $\mu \le \mu_{cr}$.

During mixing the droplet sizes r and their concentration N are changing. Therefore, as follows from Eq. (16) τ_p will be changing as well. Figure 16 also shows the dependence of time of phase relaxation vs. μ calculated for the final stage of inhomogeneous $\tau_p^{(i)}$ (dashed blue) and homogeneous $\tau_p^{(h)}$ (solid blue) mixing, and the initial stage homogeneous mixing before droplet evaporation $\tau_{pm}^{(h)}$ (blue thin line). As seen from Fig. 16 $\tau_{p0} \le \tau_{pm}^{(h)} \le \tau_p^{(h)} \le \tau_p^{(i)}$.

The humidity equilibrating time for the population of homogeneously mixed droplets $\tau_{eq}^{(h)}$ was calculated as a time when saturation ratio changed from S_{m0} to 0.999. The calculations were performed with the help of a system of differential equations. As seen from Fig. 16 $\tau_{eq}^{(h)} > \tau_p^{(h)} > \tau_{pm}^{(h)}$. The time of phase relaxation results from a solution of the Squires equation for supersaturation (Squires, 1952) as a characteristic time of approaching supersaturation to its quasi-state value S_{qs}, and in general case $\tau_p^{(h)} \neq \tau_{eq}^{(h)}$. For the case in Fig. 16 the values of $\tau_{eq}^{(h)}$ and $\tau_{pm}^{(h)}$ may differ by more than an order of magnitude, and for this specific case their ratio varies in the range $0 < \tau_{eq}^{(h)}/\tau_{pm}^{(h)} < 15$.

ACPD
15, 30211–30267, 2015

Note, that it is possible that $\tau_{eq}^{(h)} \leq \tau_{pm}^{(h)}$, when $S \rightarrow 1$ the equilibrating time $\tau_{eq}^{(h)} \rightarrow 0$. This presents a degenerate case when there is no difference between homogeneous and inhomogeneous mixing.

The equilibrating time for inhomogeneous mixing $\tau_{eq}^{(i)}$ was calculated for extreme inhomogeneous mixing: at the moment of time $t = \tau_{eq}^{(i)}$ (a) the entrained volume is saturated $S_2(\tau_{eq}^{(i)}) \approx 0$ and (b) the population of droplets with concentrationn_{ev} undergoes complete evaporation, i.e. $r(\tau_{eq}^{(i)}) \approx 0$. As seen from Fig. 16, $\tau_{eq}^{(i)}$ remains constant at $\mu > \mu_{cr}$. Basically in the frame of the inhomogeneous mixing concept $\tau_{eq}^{(i)}$ coincides with the time of evaporation of the population of droplets, which were transported into the entrained air. Obviously such a consideration is overly idealized and unlikely to happen in nature. This is suggestive that the consideration of $\tau_{eq}^{(i)}$ has significant limitations.

Comparisons of different characteristic times in Fig. 16 allow few conclusions about mixing. Thus, for $\mu_A < \mu \leq 1 \tau_{eq}^{(h)} < \tau_{ev0}$, i.e. the saturation of the environment occurs faster than the fastest possible evaporation time of a single droplet. This suggests that when $\mu_A < \mu \leq 1$ the feasibility of inhomogeneous mixing is low. For $\mu_{cr} < \mu < \mu_B \tau_{ev} < \tau_{eq}^{(h)}$, i.e. saturation of the entire volume takes longer due to evaporation of the droplet population than the complete evaporation of a single droplet. Compete evaporation of some droplets may occur, if the conditions in Eq. (29) are satisfied. This suggests that when $\mu_{cr} < \mu < \mu_B$ the feasibility of inhomogeneous mixing is increasing. Since during mixing elementary volumes are mixing at any μ homogeneous and inhomogeneous mixing may occur simultaneously in different parts of the mixing volume.

In the conclusion of this section it could be stated that τ_{react} can be characterized by different characteristic times (i.e. τ_{ev}, τ_{pm}, $\tau_p^{(h)}$, $\tau_p^{(i)}$, $\tau_{eq}^{(h)}$), each of which is a function of μ. The difference between these times can reach two orders of magnitude. This brings up a warning on a proper selection of τ_{react} in Da, and requirements for more studies to address this question.

ACPD
15, 30211–30267, 2015

6 Conclusions

This study analyses dependences of different moments of $f(r)$ in the frame of formalism of homogeneous and inhomogeneous mixing. The analysis was performed for the final stage of mixing based on the mass balance of vapor and liquid water and assumption of adiabatic process of mixing.

1. It is shown that for the case of extreme inhomogeneous mixing all moments of $f(r)$ are linearly related as $M_n = \alpha_{nm} M_m$ where coefficients α_{nm} are determined by adiabatic valued of M_n and M_m. This relation remains valid for progressive mixing.

2. Analytical relationships $M_n = F_{nm}(M_m)$ between the moments M_n and M_m were found for the case of homogenous mixing. It was demonstrated that the functional relationships between M_n and M_m exist only for the first stage of homogeneous mixing. The following progressive homogeneous mixing breaks the functional relationship between the moments. It was shown that the scattering of the moments M_n and M_m are limited by the lines for inhomogeneous mixing $M_n = \alpha_{nm} M_m$ and homogeneous mixing $M_n = F_{nm}(M_m)$.

3. The analysis of the dependences between N, β, LWC and $\overline{D}_3$ (i.e. M_0, M_2, M_3 and M_3/M_0) obtained from in-situ measurements of convective clouds suggests that the interaction between entrained and cloudy environments is dominated by inhomogeneous mixing. Homogeneous mixing may to become active, when the mixing fraction μ is close to critical μ_{cr}.

4. Analysis of different characteristic times related to evaporation and equilibrating of the mixing environment showed their strong dependence on the mixing fraction μ. The difference between different times may reach two orders of magnitude, which makes the selection of τ_{react} ambiguous. This raises a requirement of further studies on characterization of τ_{react} in Damköhler number. Comparisons of different

ACPD
15, 30211–30267, 2015

characteristic times suggest that within the same mixing environment depending on μ some volumes may be dominated by homogeneous mixing whereas others by inhomogeneous mixing.

Due to the various limitations and idealizations of the mixing process explored in the above discussion, this study acknowledges that the current description of the mixing process is far from complete. Since the process of mixing covers a wide range of time and spatial scales a comprehensive simulating efforts are required to achieve a better understanding of the process of mixing of colloidal systems. The following two works Pinsky et al. (2015a, b) in this series provide a more detailed analysis of evolution of droplet size distribution during homogeneous and inhomogeneous mixing.

Appendix A: List of symbols

The explanation of variables notations is provided in Table A1.

Appendix B: Liquid water deficit

The objective of this section is to find the amount of liquid water, which is required to evaporate in order to saturate the parcel formed after mixing of a cloud volume with sub-saturated entrained air.

Assume that q_{v1}, q_{v2} are the mixing vapor ratios in the cloudy and entrained parcels, respectively, and T_1, T_2 are their respective initial temperatures. First, we find the saturation ratio S_{m0} formed after instant mixing of the cloud and entrained before the cloud droplets start evaporating.

The vapor mixing ratio q_{vm} formed in the mixed volume will be

$$q_{vm} = \mu q_{v1} + (1 - \mu) q_{v2} \tag{B1}$$

ACPD
15, 30211–30267, 2015

The vapor pressure e_m in the mixed volume can be derived from Eq. (B1) by substituting $q_v = \frac{e}{p-e}\frac{R_a}{R_v}$, i.e.

$$e_m = P\frac{\mu + \frac{e_2(p-e_1)}{p(e_1-e_2)}}{\mu + \frac{(p-e_1)}{(e_1-e_2)}} \tag{B2}$$

The temperature of the mixed volume can be found from the energy conservation law

$$\mu(q_{v1}c_{pv} + c_{pa})(T_1 - T_{m0}) = (1-\mu)(q_{v2}c_{pv} + c_{pa})(T_{m0} - T_2) \tag{B3}$$

here c_{pv}, c_{pa}, are the specific heat capacitance of water vapor and dry air at constant pressure, respectively, T_1, T_2 are the initial temperatures in the first and second parcels before mixing; T_{m0}. Substituting q_{v1}, q_{v2} yields the temperature in the mixed volume

$$T_m = \frac{\mu T_1 + a(1-\mu)T_2}{\mu + a(1-\mu)} \tag{B4}$$

here

$$a = \frac{1 + \frac{c_{pv}R_a e_2}{c_{pa}R_v(p-e_2)}}{1 + \frac{c_{pv}R_a e_1}{c_{pa}R_v(p-e_1)}} \tag{B5}$$

With a good accuracy $a \cong 1$. The resulting saturation ratio after mixing the two volumes will be

$$S_{m0} = \frac{e_m}{E_S(T_{m0})} \tag{B6}$$

where $E_s(T_{m0})$ is the saturated vapor pressure at temperature T_{m0}.

ACPD
15, 30211–30267, 2015

If the initial saturation ratio is $S_{m0} < 1$, then the cloud droplets start evaporating. The process of evaporation is accompanied by changing humidity and temperature due to latent heat of vaporization. This process is described by the Eq. (C2) in Korolev and Mazin (2003). Assuming the process to be isobaric (i.e. vertical velocity $u_z = 0$) and absence of ice ($dq_i = 0$), Eq. (C2) (Korolev and Mazin, 2003) yields

$$\frac{dS}{S} = \left(\frac{1}{S} \frac{pR_v}{E_S R_a} + \frac{L^2}{c_p R_v T^2} \right) dq \tag{B7}$$

Integrating Eq. (B1) from initial humidity S_{m0} (Eq. 6) to saturation when $S = 1$, gives an expression

$$\delta q = \frac{L^2}{c_p R_v T_2^2} \ln \left(\frac{1 + \frac{E_S(T_{m0}) R_a L^2}{p c_p R_v^2 T_{m0}^2}}{1 + S_{m0} \frac{E_S(T_{m0}) R_a L^2}{p c_p R_v^2 T_{m0}^2}} \right) \tag{B8}$$

It should be noted that in Eq. (B8) the changes of temperature during droplet evaporation and related changes of the volume were neglected. The analysis of the behavior of Eq. (B8) shows that for wide range of temperatures $-30\,^{\circ}\mathrm{C} < T < 30\,^{\circ}\mathrm{C}$ the cases when the temperatures of the sub-saturated and cloud parcels $T_1 - T_2 < 10\,^{\circ}\mathrm{C}$, then Eq. (B2) is hold with high accuracy.

Figure B1 shows comparisons of modeled δq and that calculated from Eq. (B8) for three different temperatures. The model consisted in solving a system of differential equation with decremental evaporation of liquid water until saturation is reached.

As seen from Fig. B1 the agreement between modeled δq and that calculated from Eq. (B8) is quite good and does not exceed few percent at $S_0 = 0.5$. This discrepancy results from disregarding the effect of changing T on E_s during evaporation, i.e. in Eq. (B8) E_s and T are assumed to be constant. The changes of the air temperature due to the latent heat of vaporization increase with the increase of the amount evap-

ACPD
15, 30211–30267, 2015

orated water, when the initial humidity is decreasing (Fig. B1). The accuracy provided by Eq. (B2) is sufficient for the purposes of the present work.

Acknowledgement. Alexei Korolev work was supported by Environment Canada and Transport Canada. The COPE-MED project was funded by National Science Foundation grant AGS-1230292 and AGS-1230203. The contribution of Mark Pinsky and Alex Khain was supported by the Israel Science Foundation (grant 1393/14), the Office of Science (BER), US Department of Energy Award DE-SC0006788 and the Binational US-Israel Science foundation (grant 2010446).

References

Andejchuk, M., Grabowski, W. W., Malinowski, S. P., and Smolarkiewicz, P. K.: Numerical simulation of cloud–clear air interfacial mixing: homogeneous vs. inhomogeneous mixing., J. Atmos. Sci., 66, 2493–2500, 2009.

Baker, M. B. and Latham, J.: The evolution of droplet spectra and the rate of production of embryonic raindrops in small cumulus clouds, J. Atmos. Sci., 36, 1612–1615, 1979.

Baker, M. B. and Latham, J.: A diffusive model of the turbulent mixing of dry and cloudy air, Q. J. R. Met. Soc., 108, 871–898, 1982.

Baker, M. B., Corbin, R. G., and Latham, J.: The influence of entrainment on the evolution of cloud droplet spectra: I. A model of inhomogeneous mixing, Q. J. Roy. Meteor. Soc., 106, 581–598, 1980.

Bohren, C. F. and Albrecht, C. H.: Atmospheric Thermodynamics, Oxford University Press, New York, 402 pp., 1998.

Bower, K. N. and Choularton, T. W.: The effects of entrainment on the growth of droplets in continental cumulus clouds, Q. J. Roy. Meteor. Soc., 114, 1411–1434, 1988.

Burnet, F. and Brenguier, J. L.: Observational study of the entrainment-mixing process in warm convective clouds, J. Atmos. Sci., 64, 1995–2011, 2007.

Devenish, B. J., Bartello, P., Brenguier, J.-L., Collins, L. R., Grabowski, W. W., Ijzermans, R. H. A., Malinovski, S. P., Reeks, M. W., Vassilicos, J. C., Wang, L- P., and Warhaft, Z.: Droplet growth in warm turbulent clouds, Q. J. Roy. Meteor. Soc., 138, 1401–1429, 2012.

Dimotakis, P. E.: Turbulent mixing, Annu. Rev. Fluid Mech., 37, 329–356, 2005.

ACPD
15, 30211–30267, 2015

Gerber, H., Frick, G., Jensen, J. B., and Hudson, J. G.: Entrainment, mixing, and microphysics in trade-wind cumulus, J. Meteorol. Soc. Jpn., 86, 87–106, 2008.
Hill, T. A. and Choularton, T. W.: An airbone study of the microphysical structure of cumulus clouds, Q. J. Roy. Meteor. Soc., 111, 517–544, 1985.
Jeffery, C. A.: Inhomogeneous cloud evaporation, invariance, and Damköhler number, J. Geoph. Res., 112, D24S21, doi:10.1029/2007JD008789, 2007.
Jensen, J. and Baker, M.: A simple model of droplet spectra evolution during turbulent mixing, J. Atmos. Sci., 46, 2812–2829, 1989.
Korolev, A. V. and Filed, P. R.: The effect of dynamics on mixed-phase clouds: theoretical considerations, J. Atmos. Sci., 65, 66–86, 2008.
Korolev, A. V. and Isaac, G. A.: Drop growth due to high supersaturation caused by isobaric mixing, J. Atmos. Sci., 57, 1675–1685, 2000.
Krueger, S., Su, C.-W., and McMurtry, P.: Modeling entrainment and finescale mixing in cumulus clouds, J. Atmos. Sci., 54, 2697–2712, 1997.
Kumar, B., Schumacher, J., and Shaw, R. A.: Cloud microphysical effects of turbulent mixing and entrainment, Theor. Comput. Fluid Dyn., 27, 361–376, 2013.
Lasher-Trapp, S. G., Cooper, W. A., and Blyth, A. M.: Broadening of droplet size distributions from entrainment and mixing in a cumulus cloud, Q. J. Roy. Meteor. Soc., 131, 195–220, 2005.
Latham, J. and Reed, R. L.: Laboratory studies of the effects of mixing on the evolution of cloud droplet spectra, Q. J. Roy. Meteor. Soc., 103, 297–306, 1977.
Lehmann, K., Siebert, H., and Shaw, R. A.: Homogeneous and inhomogeneous mixing in cumulus clouds: dependence on local turbulence structure, J. Atmos. Sci., 66, 3641–3659, 2009.
Leon, D. C., French, J. R., Lasher-Trapp, S., Blyth, A. M., Abel, S. J., Ballard, S., Bennett, L. J., Bower, K., Brooks, B., Brown, P., Choularton, T., Clark, P., Collier, C., Crosier, J., Cui, Z., Dufton, D., Eagle, C., Flynn, M. J., Gallagher, M., Hanley, K., Huang, Y., Kitchen, M., Korolev, A., Lean, H., Liu, Z., Marsham, J., Moser, D., Nicol, J., Norton, E. G., Plummer, D. Price, J., Ricketts, H., Roberts, N., Rosenberg, P. D., Taylor, J. W., Williams, P. I., and Young, G.: The Convective Precipitation Experiment (COPE): investigating the origins of heavy precipitation in the southwestern UK, B. Am. Meteorol. Soc., in press, 2015.
Paluch, I. R.: Mixing and the droplet size spectrum: generalizations from the CCOPE data, J. Atmos. Sci., 43, 1984–1993, 1986.

ACPD
15, 30211–30267, 2015

Paluch, I. R. and Baumgardner, D. G.: Entrainment and fine-scale mixing in a continental convective cloud, J. Atmos. Sci., 46, 261–278, 1989.
Paluch, I. R. and Knight, C. A.: Mixing and evolution of cloud droplet size spectra in a vigorous continental cumulus, J. Atmos. Sci., 41, 1801–1815, 1984.
Pinsky, M., Khain, A., Korolev, A., and Magaritz-Ronen, L.: Theoretical investigation of mixing in warm clouds – Part 2: Homogeneous mixing, Atmos. Chem. Phys. Discuss., 15, 30269–30320, doi:10.5194/acpd-15-30269-2015, 2015.
Pinsky, M., Khain, A., and Korolev, A.: Theoretical analysis of mixing in liquid clouds – Part 3: Inhomogeneous mixing, Atmos. Chem. Phys. Discuss., 15, 30321–30381, doi:10.5194/acpd-15-30321-2015, 2015.
Rogers, R. R.: A Short Course in Cloud Physics, Pergamon press, Oxford, 227 pp., 1976.
Su, C.-W., Krueger, S. K., McMurtry, P. A., and Austin, P. H.: Linear eddy modeling of droplet spectral evolution during entrainment and mixing in cumulus clouds, Atmos. Res., 47–48, 41–58, 1998.

ACPD
15, 30211–30267, 2015

Table 1. Evaporating time (t_{ev}), evaporating distance of a free falling droplet (λ_{ev}), size of the volume (λ_υ) saturated by a completely evaporated droplet with radius r and saturation ratio S. T = 0C, P = 687 mb.

r	2 µm			5 µm			10 µm		
S	t_{ev} (s)	λ_{ev} (mm)	λ_υ (mm)	t_{ev} (s)	λ_{ev} (mm)	λ_υ (mm)	t_{ev} (s)	λ_{ev} (mm)	λ_υ (mm)
0.9	0.32	0.10	0.51	1.8	3.8	1.3	6.9	59.4	2.6
0.7	0.11	0.03	0.35	0.60	1.3	0.87	2.3	19.8	1.7
0.5	0.06	0.02	0.29	0.36	0.76	0.72	1.4	11.9	1.4
0.2	0.04	0.01	0.24	0.23	0.48	0.59	0.9	7.4	1.2

ACPD
15, 30211–30267, 2015

Table A1. List of Symbols.

Symbol	Description	Units
b	$\frac{4\pi\rho_w}{\rho_a}\frac{\frac{1}{q_v}+\frac{L_w^2}{c_{pv}R_vT^2}}{\frac{\rho_w L_w^2}{k_a R_v T^2}+\frac{\rho_w R_v T}{E_w(r)D_v}}$	$m^2\,s^{-1}$
c_{pa}	specific heat capacity of dry air at constant pressure	$J\,kg^{-1}\,K^{-1}$
c_{pv}	specific heat capacity of water vapor at constant pressure	$J\,kg^{-1}\,K^{-1}$
D	droplet diameter	m
Da	Damköhler number	–
D_v	coefficient of water vapor diffusion in the air	$m^2\,s^{-1}$
e	water vapor pressure	$N\,m^{-2}$
e_1	initial water vapor pressure in the cloud parcel	$N\,m^{-2}$
e_2	initial water vapor pressure in the entrained sub-saturated parcel	$N\,m^{-2}$
E_s	saturation vapor pressure above flat surface of water	$N\,m^{-2}$
F	$\left(\frac{\rho_w L_w^2}{k_a R_v T^2}+\frac{\rho_w R_v T}{E_w(r)D_v}\right)^{-1}$ coefficient in the equation droplet growth	$N\,m^{-2}$
$f(r)$	size distribution of cloud droplets normalized on unity	m^{-1}
k_a	coefficient of air heat conductivity	$J\,m^{-1}\,s^{-1}\,K^{-1}$
L_w	latent heat for liquid water	$J\,kg^{-1}$
LWC	liquid water content	$kg\,m^{-3}$
l_p	characteristic spatial phase scale	m
m_1 m_2 M_n	mass of the cloud parcel (1 kg) mass of the entrained air (1 kg) nth moment of the droplet size distribution $\frac{\int_0^\infty f(r)r^n dr}{\int_0^\infty f(r)dr}$	kg kg m^n
N N_0	concentration of droplets concentration of droplets before mixing	m^{-3} m^{-3}
p	pressure of moist air	$N\,m^{-2}$
p_a	pressure of dry air	$N\,m^{-2}$
r	droplet radius	m
$\overline{r}$	mean droplet radius	m
$\overline{r}_2$	mean square droplet radius	m
$\overline{r}_3$	mean cubic droplet radius	m
R_a	specific gas constant of moist air	$J\,kg^{-1}\,K^{-1}$
R_v	specific gas constant of water vapor	$J\,kg^{-1}\,K^{-1}$
q	cloud liquid water mixing ratio (mass of liquid water per 1 kg of dry air)	–
q_0	cloud liquid water mixing ratio before mixing	–
q_v	water vapor mixing ratio (mass of water vapor per 1 kg of dry air)	–
S	e/E_S, relative humidity over water (saturation ratio)	–
S_m	relative humidity after mixing is completed	–

ACPD
15, 30211–30267, 2015

Table A1. Continued.

Symbol	Description	Units
S_{m0}	relative humidity after instant mixing of cloudy and entrained air but before droplets evaporation	–
T	temperature	K
T_1	temperature of the cloud parcel before mixing	K
T_2	temperature of the entrained sub-saturated parcel before mixing	K
T_{m0}	temperature of the parcel after vapor mixing, but before droplet evaporation	K
t	Time	s
u_z	vertical velocity	m s^{-1}
β	extinction coefficient	m^{-1}
β_0	extinction coefficient before mixing	β_0
δq	amount of liquid water per 1 kg of sub-saturated air required to saturate the air in the mixed parcel before droplet evaporation Eq. (5)	–
δq^*	amount of liquid water per 1 kg of dry air required to saturate the air in the entrained cloud free volume Eq. (8)	–
ε	turbulent energy dissipating rate	m^2 s^3
μ	mixing fraction of cloud and dry parcels $0 \le \mu \le 1$	–
μ_{cr}	critical mixing fraction, such that for $\mu \le \mu_{cr}$ all droplets evaporate	–
ρ_a	density of the dry air	kg m^{-3}
ρ_w	density of liquid water	kg m^{-3}
τ_{ev}	time of complete evaporation	s
τ_{ev}	time of complete evaporation at constant $S = S_{m0}$	s
τ_{ev0}	time of complete evaporation at constant $S = S_2$	s
$\tau_{eq}^{(h)}$	time of saturating environment during evaporation of a population of homogeneously mixed droplets	s
$\tau_{eq}^{(i)}$	time of saturating environment for a population of inhomogeneously mixed droplets	s
τ_p	time of phase relaxation	s
$\tau_p^{(h)}$	time of phase relaxation after completing homogeneous mixing	s
$\tau_p^{(i)}$	time of phase relaxation after completing inhomogeneous mixing	s

ACPD
15, 30211–30267, 2015

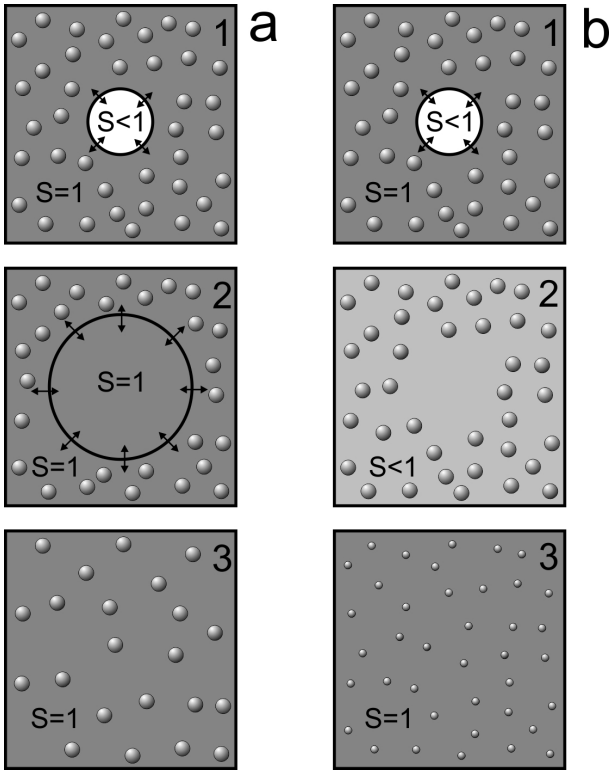

Figure 1. Classical conceptual diagram of **(a)** inhomogeneous and **(b)** homogeneous mixing. (1) initial state; (2) mixing state; (3) final state.

ACPD
15, 30211–30267, 2015

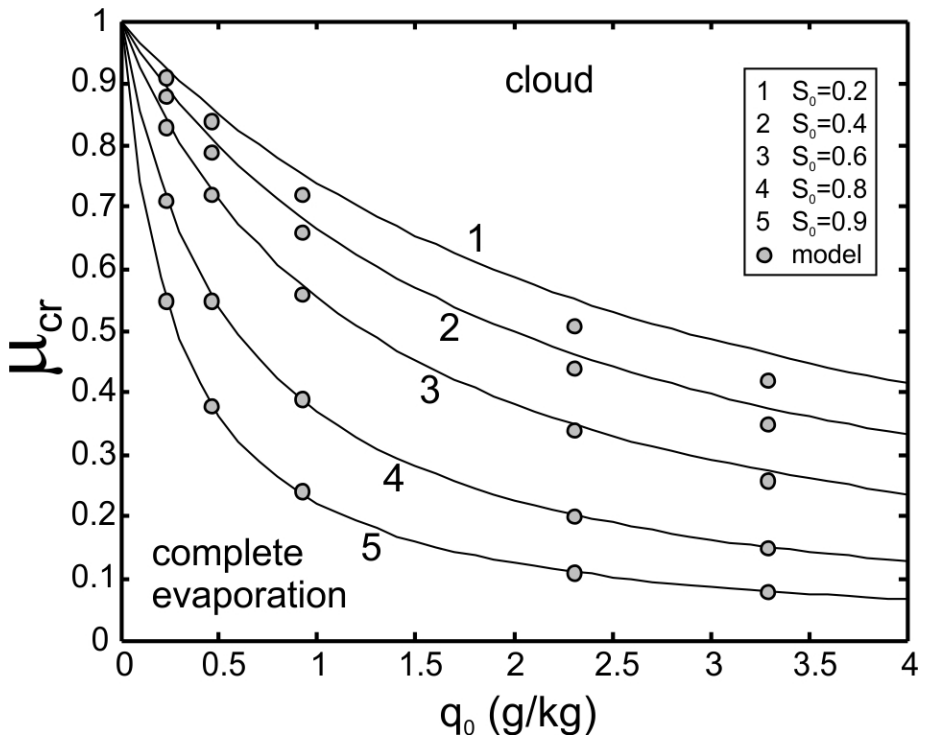

Figure 2. Dependence of initial ratio of mixing q_0 vs. critical ratio of mixing μ_{cr} calculated from Eq. (23). Circles indicate modeled points. The calculations were performed for $T = 0\,^{\circ}\mathrm{C}$ and $H = 3000\,\mathrm{m}$.

ACPD
15, 30211–30267, 2015

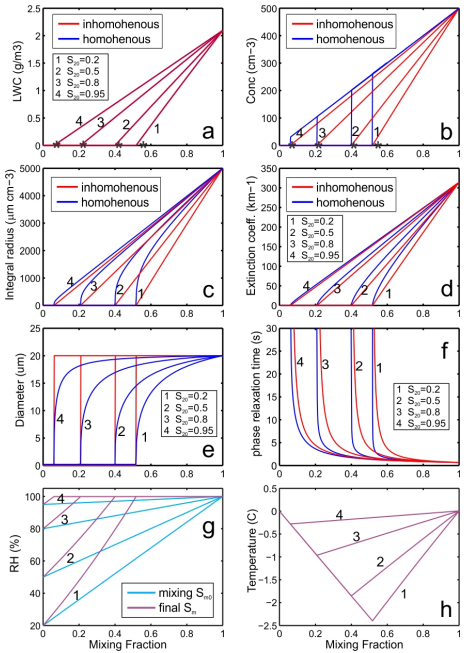

Figure 3. Simulation of **(a)** droplet number concentration and **(b)** liquid water mixing ratio, **(c)** integral droplet radius, **(d)** extinction coefficient, **(e)** mean cube diameter, **(f)** time of phase relaxation, **(g)** relative humidity in the mixed volume before droplet evaporation S_{m0} and final S_m, **(h)** final temperature T_m vs. ratio of mixing μ formed after homogeneous and inhomogeneous mixing between dry and cloudy parcel with monodisperse droplets. Black stars on **(a)** and **(b)** indicate critical ratio of mixing μ_{cr} calculated from Eq. (23). The calculations were performed for RH_{20} = 20, 50, 80, 95 %; r_0 = 10 μm, N_0 = 500 cm^{-3}; $T_{10} = T_{20}$ = 0 °C; H = 1000 m.

ACPD
15, 30211–30267, 2015

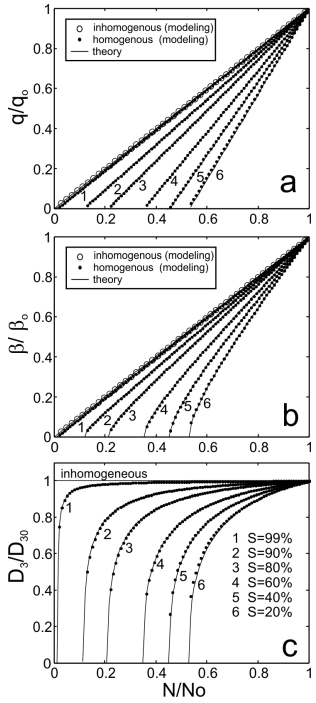

Figure 4. Dependence of normalized mixing ratio q/q_0, extinction coefficient β/β_0 and mean volume diameter r_3/r_0 vs. normalized number concentration N/N_0. The calculations were performed for different relative humidity of the entrained air RH: (1) 99 %; (2) 90 %; (3) 80 %; (4) 60 %; (5) 40 %; (6) 20 %. The initial conditions used for the calculations were: H_0 = 1000 m; T_1 (0)= T_2 (0)= 0 °C; r_0 = 10 µm, N_0 = 500 cm^{-3}.

ACPD
15, 30211–30267, 2015

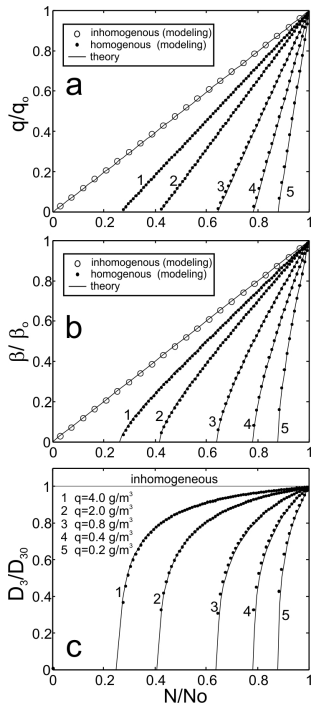

Figure 5. Effect of the water content q_0 on mixing. Same as in Fig. 4. The calculations were performed for different initial liquid water content: (1) 4.0 g kg^{-1}; (2) 2.0 g kg^{-1}; (3) 0.8 g kg^{-1}; (4) 0.4 g kg^{-1}; (5) 0.2 g kg^{-1}. The initial conditions used for the calculations were: H_0 = 1000 m; RH(0) = 50 %; T_1 (0) = T_2 (0) = 0 °C; r_0 = 10 µm.

ACPD
15, 30211–30267, 2015

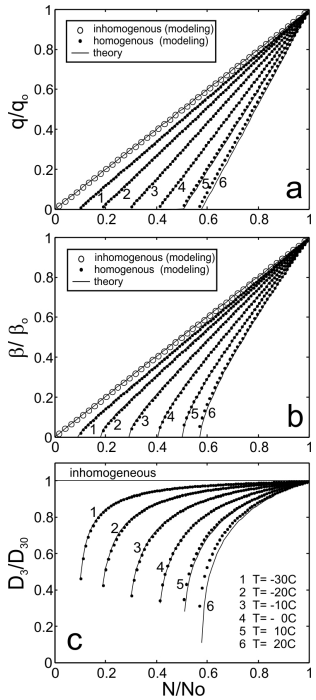

Figure 6. Effect of temperature on mixing. Same as in Fig. 4. The calculations were performed for different initial temperatures T: (1) −30 °C; (2) −20 °C; (3) −10 °C; (4) 0 °C; (5) 10 °C; (6) 20 °C. The initial conditions used for the calculations were: H_0 = 1000 m, RH(0) = 50 %; r_0 = 10 µm, N_0 = 500 cm^{-3}.

ACPD
15, 30211–30267, 2015

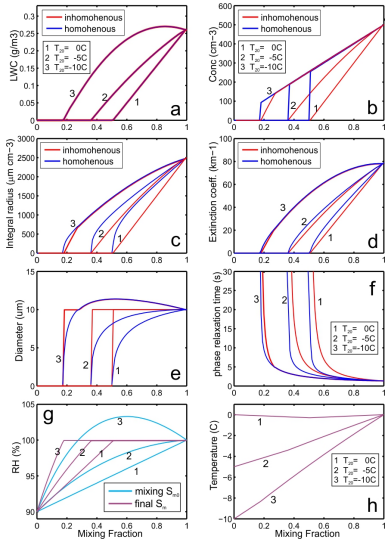

Figure 7. Simulation of **(a)** droplet number concentration and **(b)** liquid water mixing ratio, **(c)** integral droplet radius, **(d)** extinction coefficient, **(e)** mean cube diameter, **(f)** time of phase relaxation, **(g)** relative humidity in the mixed volume before droplet evaporation S_{m0} and final S_m, **(h)** final temperature T_m vs. ratio of mixing μ formed after homogeneous and inhomogeneous mixing between dry and cloudy parcel with monodisperse droplets. Black stars on **(a)** and **(b)** indicate critical ratio of mixing μ_{cr} calculated from Eq. (22). The calculations were performed for RH = 90 %; r_0 = 5 μm; N_0 = 500 cm^{-3}; T_{10} = 0 °C; T_{20} = −10, −5, 0 °C; H = 1000 m.

ACPD
15, 30211–30267, 2015

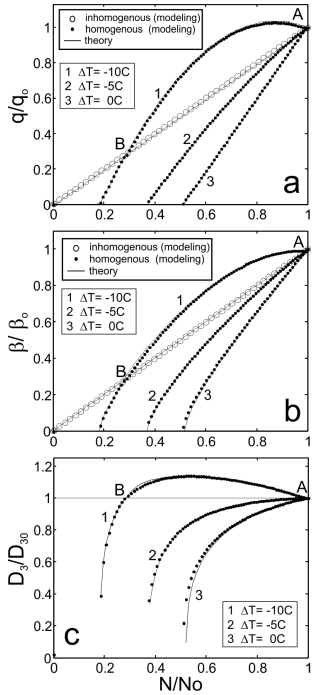

Figure 8. Effect of temperature difference between cloud and entrained air on mixing. Same as in Fig. 4. The calculations were performed for different initial temperatures ΔT: (1) −10 °C; (2) −5 °C; (3) −0 °C. The initial conditions used for the calculations were: H_0 = 1000 m, RH(0) = 90 %; r_0 = 5 µm; N_0 = 500 cm^{-3}; T_{10} = 0 °C.

ACPD
15, 30211–30267, 2015

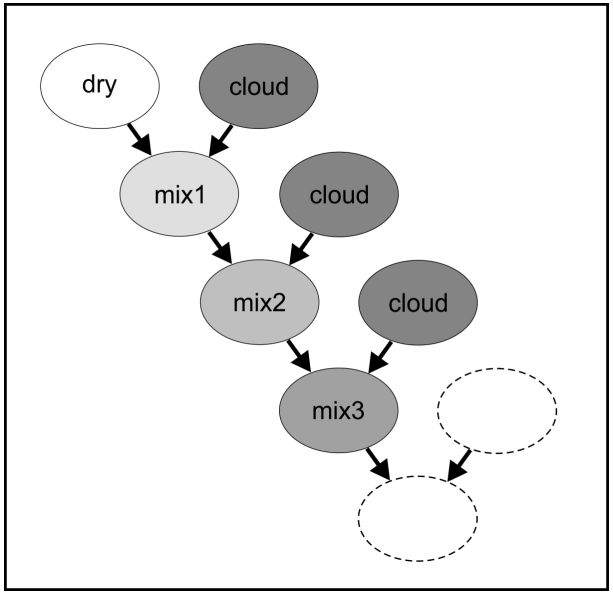

Figure 9. Conceptual diagram of cascade mixing of the out-of-cloud entrained parcel with the cloudy environment.

ACPD
15, 30211–30267, 2015

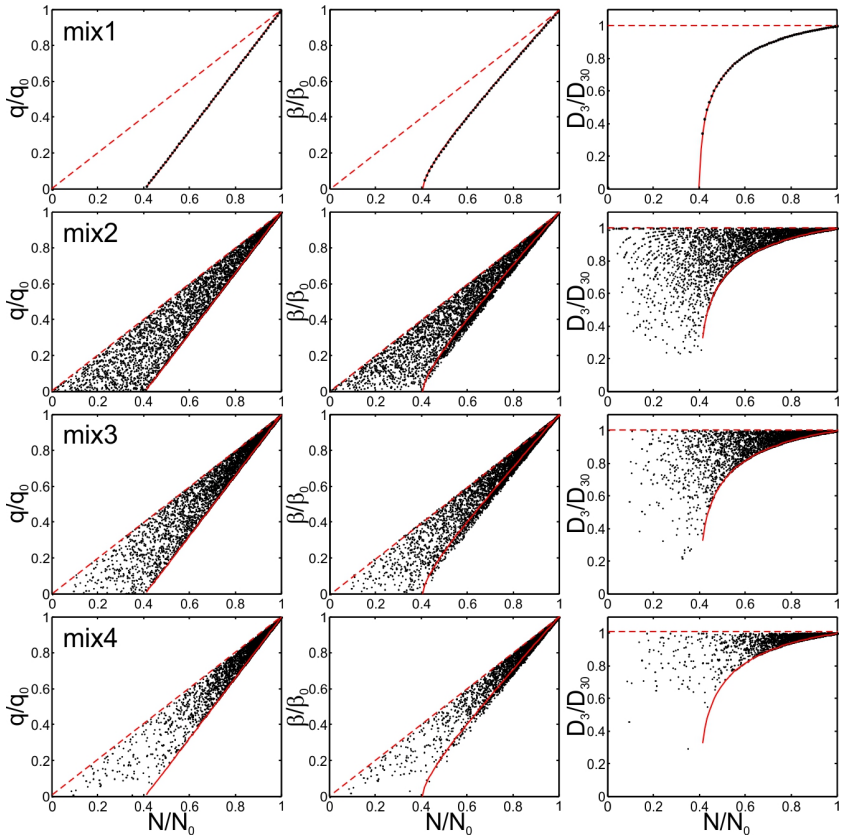

Figure 10. Simulation of stochastic mixing corresponding to stages 1–4 as indicated in Fig. 7. Solid red lines indicate the dependences q, β, $\overline{D}_3$ vs. N for the primary stage. Dashed red lines indicate the same dependences for inhomogeneous mixing. The initial conditions used for the simulations were: H_0 = 1000 m, T_1 (0) = T_2 (0) = 0 °C; RH_2 (0) = 50 %; r_0 = 10 µm, N_0 = 500 cm^{-3}.

ACPD
15, 30211–30267, 2015

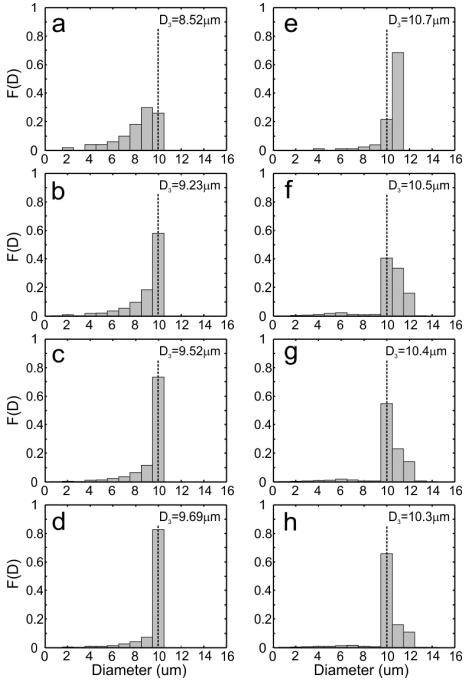

Figure 11. Droplet size distributions formed during the progressive homogeneous mixing corresponding to the **(a, e)** primary stage; **(b, f)** 2nd stage; **(c, g)** 3rd stage; **(d, h)** 4th stage. Left column **(a, b, c, d)** corresponds to the case when the cloud temperature is equal to the dry air temperature $T_{10} = T_{20} = 0\,^{\circ}\mathrm{C}$, right column **(e, f, g, h)** corresponds to the case when the dry air temperature is colder than that of cloud $T_{10} = 0\,^{\circ}\mathrm{C}$; $T_{20} = -10\,^{\circ}\mathrm{C}$. For both cases the simulation was performed for $r_0 = 5\,\mu\mathrm{m}$; $N = 500\,\mathrm{cm}^{-3}$; $\mathrm{RH}_2\ (0) = 90\,\%$.

ACPD
15, 30211–30267, 2015

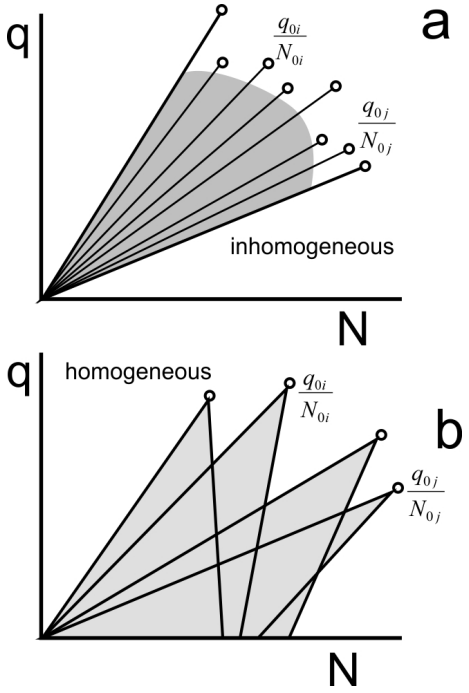

Figure 12. Conceptual diagrams of scattering of measurements of q vs. N for **(a)** extreme inhomogeneous and **(b)** homogeneous mixing.

ACPD
15, 30211–30267, 2015

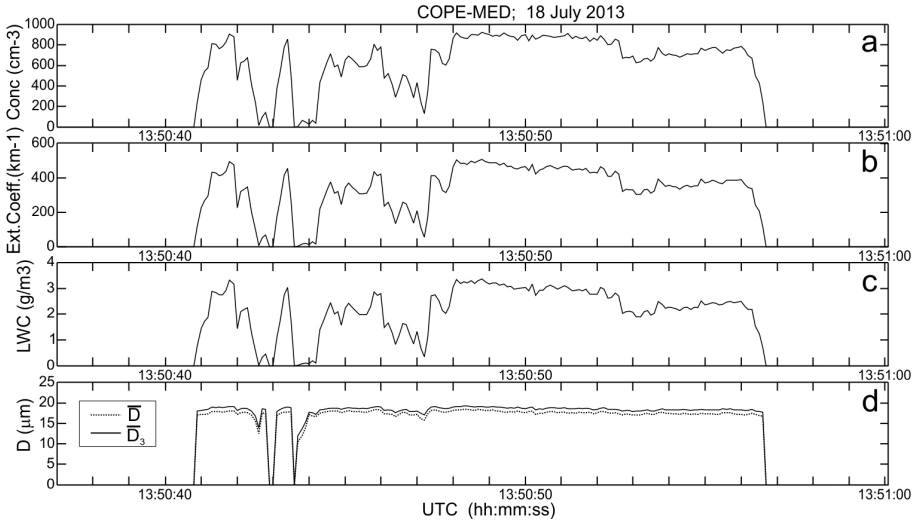

Figure 13. Spatial changes of particle concentration **(a)**, extinction coefficeint **(b)**, liquid water content **(c)** and average and mean mass diameter **(d)** during transit through one of the convective clouds measured by CDP. The measurements were conducted during the COPE-MED project on 18 July 2015. The sampling rate 10 Hz (~ 10 m spatial resolution). H = 5500 m; T = −120 °C; RH = 20 %.

ACPD
15, 30211–30267, 2015

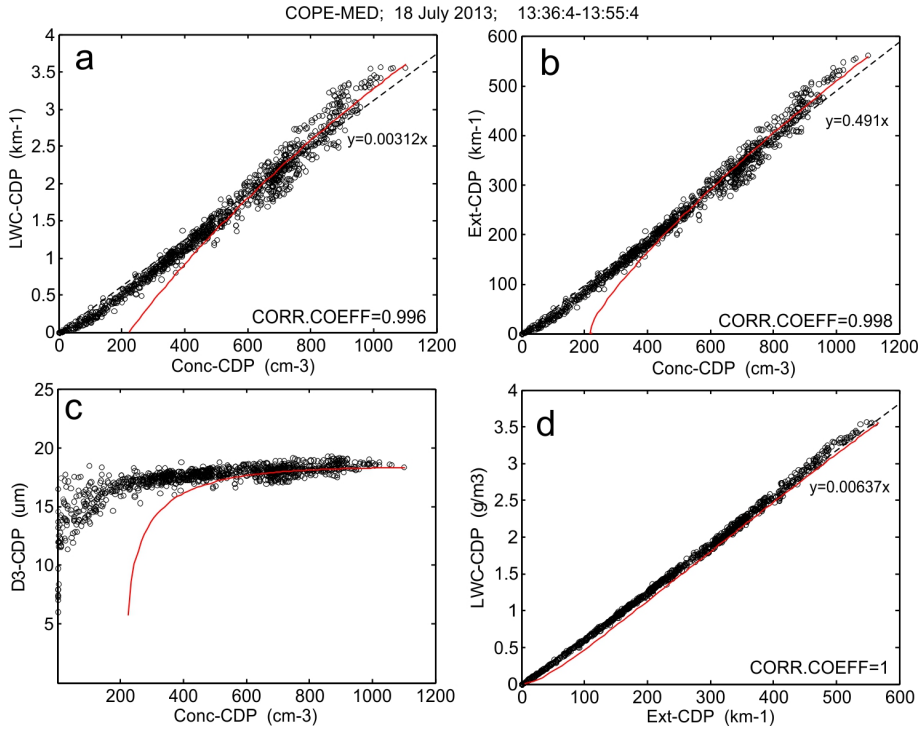

Figure 14. Relatonships between **(a)** LWC(N); **(b)** $\beta(N)$; **(c)** $\overline{D}_3(N)$; **(d)** LWC(β) calculated from the CDP measurements obtained during sampling several convective clouds. The meadurements were conducted during the COPE-MED project on 18 July 2015, $H = 5500$ m; $T = -12\,^{\circ}$C; RH = 20 %. The measurements were sampled at 10 Hz ($\sim$ 10 m spatial resolution).

ACPD
15, 30211–30267, 2015

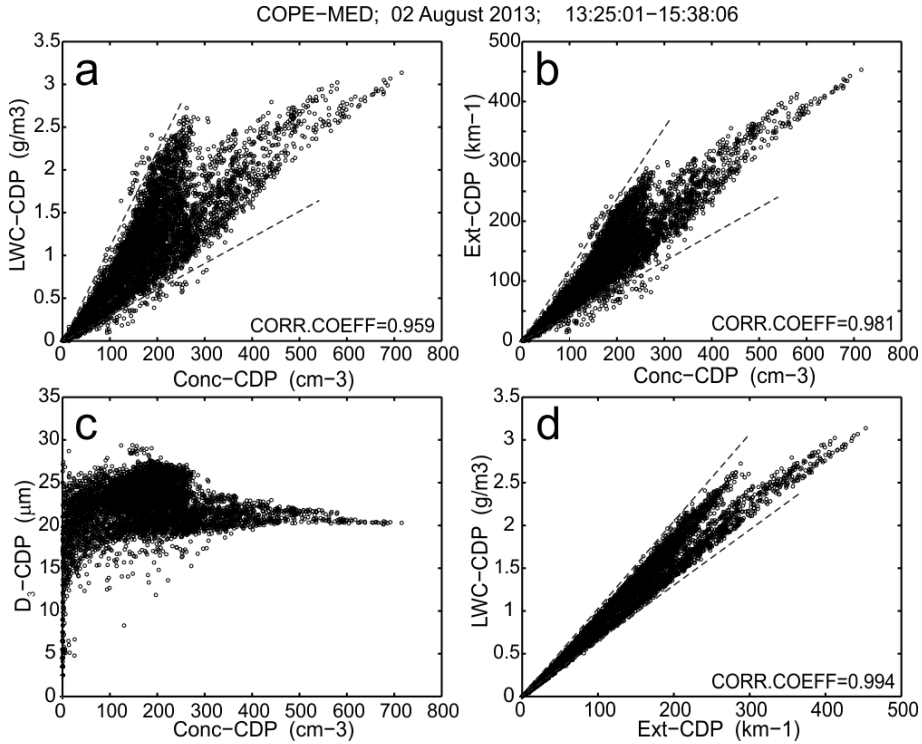

Figure 15. Relatonships between **(a)** LWC(N); **(b)** $\beta(N)$; **(c)** $\overline{D}_3(N)$; **(d)** LWC(β) calculated from the CDP measurements sampled during traverse through 45 convective clouds. The meadurements were conducted during the COPE-MED project on 2 August 2015. Dashed lines indicate **(a)**, **(b)** and **(d)** indicate the sectors, where the majority of the points are scattered. The altitude of sampling varied in the range 3000 m $< H <$ 4500 m, temperature $-11\,^{\circ}\mathrm{C} < T < 0\,^{\circ}\mathrm{C}$, relative humidity in the vicinity of clouds 15 % < RH < 65 %. The measurements were sampled at 10 Hz ($\sim$ 10 m spatial resolution).

ACPD
15, 30211–30267, 2015

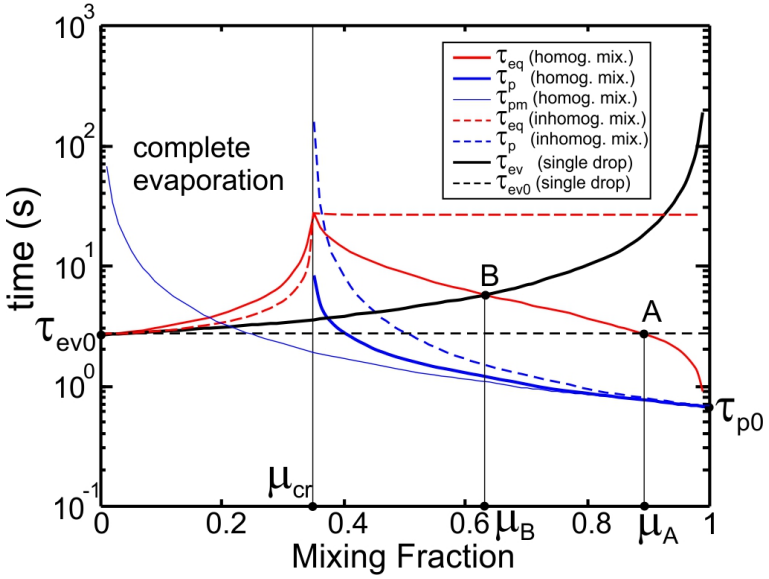

Figure 16. Dependencies of different characteristic times vs. ratio of mixing. The calculations were performed for RH_{20} = 50 %; r_0 = 10 µm, N_0 = 500 cm^{-3}; $T_{10} = T_{20}$ = 0 °C; H = 1000 m.

ACPD
15, 30211–30267, 2015

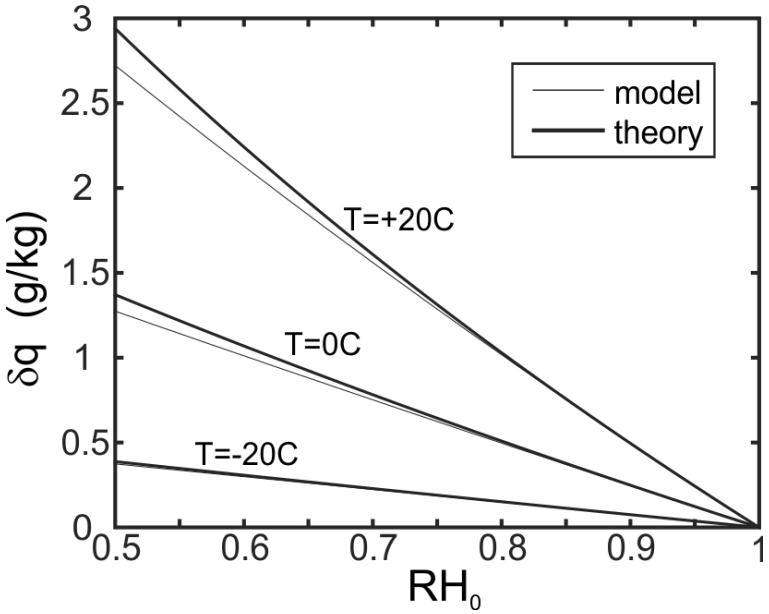

Figure 17. Amount of evaporated liquid water δq required for saturation of a cloud volume with initial humidity RH_0. Comparisons of the modeled δq and that calculated from Eq. (B8) for three different temperatures −20, 0 and 20 °C. Calculations were performed for P = 880 mb.

ACPD
15, 30211–30267, 2015